This is manuscript version of the paper „Straka F., Schornik D., Masin J., Filova E., Mirejovsky T., Burdikova Z., Svindrych Z., Chlup H., Horny L., Daniel M., Machac J., Skibová J., Pirk J., Bacakova L. (2018) A human pericardium biopolymeric scaffold for autologous heart valve tissue engineering: cellular and extracellular matrix structure and biomechanical properties in comparison with a normal aortic heart valve. Journal of Biomaterials Science Polymer Edition.“ Link to the Publisher version: http://www.tandfonline.com/doi/abs/10.1080/09205063.2018.1429732

# A human pericardium biopolymeric scaffold for autologous heart valve tissue engineering: cellular and extracellular matrix structure and biomechanical properties in comparison with a normal aortic heart valve

Frantisek Straka, David Schornik, Jaroslav Masin, Elena Filova, Tomas Mirejovsky, Zuzana Burdikova, Zdenek Svindrych, Hynek Chlup, Lukas Horny, Matej Daniel, Jiri Machac, Jelena Skibová, Jan Pirk and Lucie Bacakova

**Abstract**: The objective of our study was to compare the cellular and extracellular matrix (ECM) structure and the biomechanical properties of human pericardium (HP) with the normal human aortic heart valve (NAV). HP tissues (from 12 patients) and NAV samples (from 5 patients) were harvested during heart surgery. The main cells in HP were pericardial interstitial cells, which are fibroblast-like cells of mesenchymal origin similar to the valvular interstitial cells in NAV tissue. The ECM of HP had a statistically significantly ($p < 0.001$) higher collagen I content, a lower collagen III and elastin content, and a similar glycosaminoglycans (GAGs) content, in comparison with the NAV, as measured by ECM integrated density. However, the relative thickness of the main load- bearing structures of the two tissues, the dense part of fibrous HP (49 ± 2%) and the lamina fibrosa of NAV (47 ± 4%), was similar. In both tissues, the secant elastic modulus (Es) was significantly lower in the transversal direction ($p < 0.05$) than in the longitudinal direction. This proved that both tissues were anisotropic. No statistically significant differences in UTS (ultimate tensile strength) values and in calculated bending stiffness values in the longitudinal or transversal direction were found between HP and NAV. Our study confirms that HP has an advantageous ECM biopolymeric structure and has the biomechanical properties required for a tissue from which an autologous heart valve replacement may be constructed.

## 1. Introduction

It is estimated that around 300 000 heart valve replacements are implanted worldwide each year, and this number will increase over the next few decades [1]. Most of them are aortic valve replacements, more than 200000 of which are performed annually. The morbidity and mortality of isolated aortic valve replacements have fallen, despite the gradual rise in patient age and in the overall risk profile [2]. There has been an important shift toward the use of bioprosthetic heart valve replacements in recent years [2].

All currently available forms of valve replacements have several inherent problems in their design. Mechanical prostheses are composed of pyrolytic carbon or titanium, and have an estimated lifespan of 25 years. Biological heart valve replacements are made from chem- ically crosslinked bovine pericardium, porcine aortic heart valves or allogeneic cadaveric cryopreserved valves, and have an estimated functional lifespan of around 15 years. These valve prostheses are predisposed to infection, thrombus formation, calcification, fibrosis, degenerative changes and deterioration [3,4]. At the present time, only autologous pulmo- nary heart valve implantation into the aortic position (the Ross procedure) has produced a functional autologous heart valve replacement in humans [5]. However, this is a difficult operation with a high early mortality rate (up to 10%). It involves a concomitant pulmonary heart valve replacement procedure, and is complicated by valve stenosis of the homograft in long-term follow-up [5].

A challenge in heart valve tissue engineering has been to create an autologous heart valve prosthesis that will have a similar structure and similar biomechanical properties to the normal heart valve. The goal is to design a heart valve prosthesis that is also free of valve-related complications, which is non-immunogenic, which has the potential to regenerate, and which is devoid of foreign synthetic materials and toxic substances, such as glutaraldehyde-fixed xenogeneic or allogeneic tissues [3,6]. Several approaches have been described in the preparation of tissue-engineered heart valves (TEHVs), using a variety of biocompatible synthetic polymer scaffolds such as poly(glycolic acid) [(PGA)], poly(lactic acid) [(PLA)], poly(e-caprolactone) [(PCL)], poly(4-hydroxybutyrate) [(P4HB)], polyu- rethane (PU), or polyhydroxyoctanoate [(PHO)], and using various techniques, such as decellularization of biological materials, molded or sutured scaffolds, 3D bioprinting, elec- trospinning, stereolithography, hybrid techniques and in vivo self-assembly molding [3]. A variety of cells have been used for seeding the

scaffolds, e.g. vascular-derived smooth muscle cells (VSMCs), mesenchymal stem cells (MSCs), valvular interstitial cells (VICs) and fibroblasts. However, the clinical utility of these prostheses has been limited by inappropriate micro-architecture, immune-mediated graft degeneration, incomplete recellularization or decellularization and graft failure at systemic pressures, resulting in deformation under stress [3]. The use of a non-autologous tissue can also cause an unwanted negative immune response after implantation. This can lead to the development of degenerative changes, and to valve failure typical of xenogeneic TEHVs [6].

An optimal autologous scaffold for heart valve tissue engineering should attempt to mimic the ECM structure of the normal human heart valve, including the collagen, elastin and glycosaminoglycans (GAGs) content [3,7]. It should also have similar biomechanical properties to the normal aortic valve (NAV) [3]. Autologous human pericardium (HP) has the potential to meet these conditions. The HP forms a sac around the heart containing a small amount of serous fluid (about 20 ml) that surrounds the heart and the proximal portion of the great vessels [8]. HP is the external part of the pericardial sac. It consists of an outer layer called the fibrous pericardium, which anchors the heart to the mediastinum, and an inner layer called the serous pericardium, which is lined by squamous mesothelial cells producing the pericardial fluid. The main function of HP is to limit overfilling of the heart chambers, and to form a barrier to prevent the spread of infection from adjacent structures of the mediastinum [8]. Although the pericardium sac is usually opened during cardiac surgery, HP is not routinely used in the creation of TEHVs. Only a small number of studies have described its use for the reconstruction or replacement of heart valves in patients with heart valve disease [9,10].

The objective of our study was therefore to perform a detailed evaluation and comparison of the cellular and ECM structure and the biomechanical properties of HP and of human NAV tissues. A morphological analysis needs to be made, and the stratification of the tissue layers needs to be studied, in order to understand the native function of the two tissues. Histological and immunohistochemical evaluations were therefore carried out. We charac- terized the biopolymeric structure and investigated the cellular and ECM interaction of the two tissues, using environmental scanning electron microscopy (ESEM), second harmonic generation confocal microscopy (SHG) and two-photon excitation microscopy (TPEM) with CMFDA (5-chloromethylfluorescein diacetate) staining of living cells. Histomorphometric measurements were used to quantify the biopolymer content of ECM and to clarify the mechanical contribution of collagen I, III, elastin and GAGs to the tensile behavior of HP and NAV. The biomechanical properties of both tissues were evaluated with uniaxial tensile testing. Finally, we discuss the possibility of harvesting autologous HP by minimally invasive procedures, and we comment on earlier clinical studies in which autologous HP has been used as a scaffold for the reconstruction of heart valves or for creating TEHV replacements.

## 2. Materials and methods

### 2.1 Study group and tissue harvesting

Our study group consists of 17 patients (tissue donors). All patients signed an informed consent form prior to enrolment in the study. The project was approved by the Ethical Committee of the Institute for Clinical and Experimental Medicine in Prague, Czech Republic. Native HP samples, approximately 4 × 10 cm in size, were harvested at the time of heart surgery from the anterior part of the heart from 12 patients (undergoing coronary artery bypass grafting or valve surgery, 2 women, 10 men, average age 67 ± 7 years). Fatty tis- sues with a heavy vasculature were removed from the samples. NAV samples were obtained from 5 other patients (5 men with dilated cardiomyopathy, average age 51 ± 15 years) during heart transplantation. The tissue samples were obtained at different times, depending on the scheduled surgery (Figure 1), and were transported to the laboratory in a sealed container containing DMEM (Dulbecco’s Modified Eagle’s Medium; Sigma, St. Louis, MO, U.S.A; Cat. No. D5648) at body temperature (37 °C).

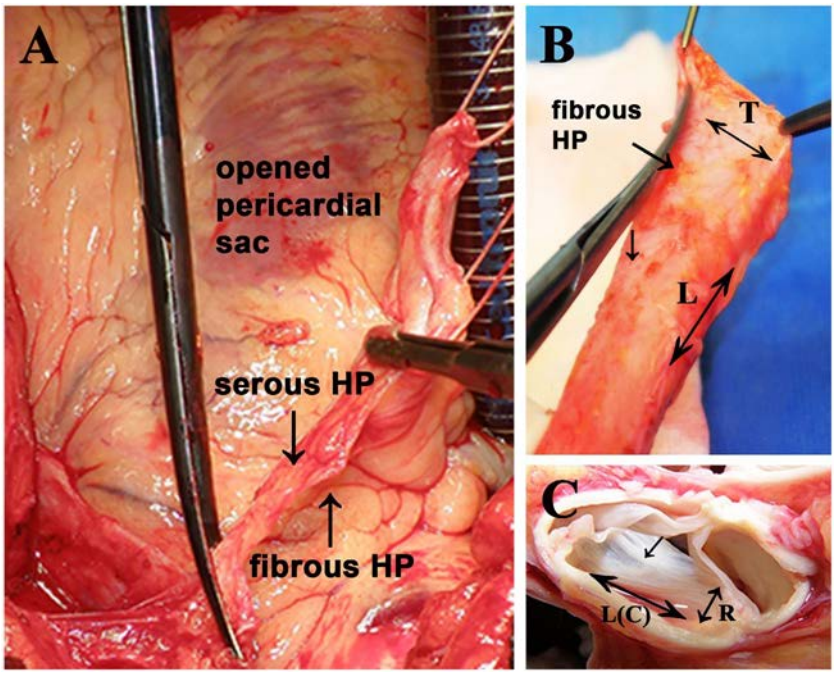


**Figure 1.** method. tissues were harvested during open heart surgery. after opening the pericardial sac, a macroscopic structure of the fibrous and serous part of human pericardium (HP) was evident (arrows) – (a). HP from the anterior part of the heart, after removing fatty tissues with vasculature – (B). a normal aortic heart valve (naV) – (c). l – human pericardium in the longitudinal direction (= HP_l), t – human pericardium in the transversal direction (= HP_t), l(c) – normal (native) aortic valve in the longitudinal (circumferential) direction (= naV_l), r – normal (native) aortic valve in the radial direction (=naV_r). notes: small arrow in B – macroscopically observed collagen bundles oriented longitudinally in relation to HP harvested from the anterior part of the heart. small arrow in c – macroscopically observed collagen bundles angled downward from the commisures toward the center and in the circumferential direction, parallel to the free edge of the naV cusp.

## 2.2 Histological and immunohistochemical analysis

For the histological evaluation, the samples were fixed in 10% formalin, dehydratated and embedded in paraffin wax, cut at 4 μm and stained with Hematoxylin-eosin (H&E) and Elastica Weigert – van Gieson. Alcian blue staining was used for staining acidic glycos- aminoglycans (GAGs; mucopolysaccharides).

Immunohistochemical detection of collagen I, III and elastin was performed on paraffin sections 4 μm in thickness, using a two-step indirect method. The slides were deparaffinized in xylene, and were rehydrated in graded ethanol. After deparaffinization and rehydration, endogenous peroxidase was blocked by 0.3% H2O2 in 70% methanol for 30 min. A pri- mary antibody was applied for 30 min at RT, and antibody detection was performed using Histofine Simple Stain MAX PO (MULTI) Universal Immuno-peroxidase Polymer, anti- Mouse and anti-Rabbit (Histofine; Nichirei, Japan). Immunohistochemical detection of vimentin (a type III intermediate filament protein), desmin (a marker of striated muscles), alpha smooth muscle actin (α-SMA), Ki-67 (a nuclear marker for cell proliferation), CD31 (a platelet-endothelial cell adhesion molecule, also referred to as PECAM-1), leukocyte common antigen (LCA) and β-catenin (a cell adhesion protein associated with cadherin junctions linking cadherins to the actin cytoskeleton) were performed on sections of par- affin-embedded tissues 4 μm in thickness, using the Ventana Benchmark Ultra system (Tuscon, AZ, USA) with the ultraView Universal DAB Detection Kit.

The primary antibodies were: anti-vimentin (1:500; V9, Dako, Glostrup, Denmark), anti-α-SMA (1:1000; 1A4, Dako, Glostrup, Denmark), anti-Ki-67 (1:100; MIB1, Dako, Glostrup, Denmark), anti-CD 31(1:100; JC7OA, Dako, Glostrup, Denmark), anti-LCA (1:100; 2B11 + PD7/26, Dako, Glostrup, Denmark), anti-β catenin (1:100; 17C2, Leica Biosystems, Germany), anti-desmin (1:100; D33, Dako, Glostrup, Denmark), anti-colla- gen I (1:50; polyclonal, CosmoBio Co., Japan), anti-collagen III (1:100; FH-7A, Abcam, Cambridge, UK) and anti-elastin (1:200; polyclonal, Abcam, Cambridge, UK). Finally, the specimens were stained with Dako Liquid DAB (3.3 diaminobenzidine) + Substrate- Chromogen System (Dako, Glostrup, Denmark) for 5 min, and were then counterstained with Harris’s Hematoxylin and were mounted.

The stained specimens were evaluated by light microscopy (Leica DMLB 100S and Olympus BX 40 microscope), and microphotographs were taken (Leica Image Manager software).

### 2.3 Environmental scanning electron microscopy (ESEM)

Electron micrographs of the HP and the NAV were taken in the Environmental Scanning Electron Microscope (ESEM) mode of the FEI Quanta 200 ESEM scanning electron micro- scope (FEI Czech Republic s.r.o., Brno, Czech Republic). The images were performed from the outer (aortic) side of the NAV and from the outer side of the fibrous HP after removing the surrounding fatty tissue.

With the ESEM operating in this ‘wet’ non-high-vacuum mode, it was possible to scan the tissue surface in its natural state without the need to prepare a metal-based coating. Each specimen was carefully washed in distilled water, partially dried and placed on a metal stub of a Peltier cooling stage (JT Manufacturing, Hudson, NH, USA) in the microscope cham- ber. The stub had already been covered with a two-sided adhesive conductive carbon tape to prevent the sample drifting. Then the chamber was pumped to a pressure of ca. 300 Pa, together with the controlled addition of water vapor. In this time, the temperature of the sample was decreased below −10 °C (using the Peltier stage with an external water chiller) to achieve 100% relative humidity at the surface of the sample to protect it from dehydra- tion. The following settings were used for image acquisition: electron beam accelerating voltage of 20 kV, the Gaseous Secondary Electron Detector (GSED), with magnification up to 1000x. The transverse radius of the collagen bundles protruding beneath the HP and NAV surfaces was measured from ESEM images.

### 2.4 Second harmonic generation (SHG) and two-photon excitation microscopy (TPEM)

SHG and TPEM were used to compare the superficial structure of HP and NAV. All images were acquired by a Leica TCS SP2 acoustooptical beamsplitter (AOBS) multiphoton confocal laser scanning microscope based on the Leica DM IRE2 inverted microscope and equipped with the following light sources: an Ar laser (458 nm/5 mW, 476 nm/5 mW, 488 nm/20 mW, 514 nm/20 mW), HeNe lasers (543 nm/1.2 mW, 633 nm/10 mW) for one-photon excitation, and a mode-locked Titanium(ti) – Sapphire Chameleon Ultra laser (Coherent Inc., Santa Clara, CA, USA), tuneable from 690 to 1040 nm for TPEM.

The light emitted from collagen was detected by NDD – RLD photomultipliers installed directly under the lens of a scanning confocal microscope head. Using SHG, the collagen signal was recorded as λex (the wavelength of the excited photons) 860 nm, and λem (the wavelength of the emitted photons) 430 nm. Live cells were labelled by CellTrackerTM Green CMFDA (5-chloromethylfluorescein diacetate, Molecular Probes, Invitrogen Detection Technologies). The tissue samples were immersed in a CMFDA dye solution (at a con- centration of 10.0 μM/L in a serum-free medium) for 30 min at 37 °C in an incubator, according to the manufacturer’s instructions. CMFDA is a colorless dye that releases a brightly fluorescent product after being cleaved by the cell’s cytosolic esterases, a reaction that also involves glutathione-SH. The time management between tissue dissection and image acquisition was no longer than 45 min.

TPEM was used to assess the cell morphology, distribution, viability, cell-cell and cell-ma- trix interactions and the elastin fiber architecture [11]. SHG imaging was performed to assess the architecture and the spatial distribution of the collagen fibers [12]. Both of surfaces of the NAV cusps (lamina fibrosa and lamina ventricularis) and the HP tissue (the outer dense part and the inner serosal part of fibrous HP) were assessed to a maximal penetration depth of around 80–100 um.

In our study, temperature had the greatest impact on cell viability. A heated chamber and a heated objective were applied to optimize the temperature (37 °C) during image acquisi- tion. The arrangement and the crimped pattern of the collagen fibers were analyzed from the images that were acquired. The crimped period was measured as the distance between the crimp peaks of two neighboring collagen fibers. The crimp amplitude was measured as the perpendicular distance from the midpoint to the peak of the crimp wave of the collagen fibers. Multiple collagen fibers were evaluated for each image.

### 2.5 Quantitative tissue analysis – tissue layer stratification

A histomorphometric evaluation of the tissue layer stratification was performed using ImageJ analysis software (Image Processing and Analysis in Java; National Institute of Health, USA) [13].

Leaflet layers, as well as the percentage total thickness of lamina fibrosa (F), lamina spon- giosa (S) and lamina ventricularis (V) of the NAV and the outer dense part of the fibrous HP (Fd), the inner serosal part of the fibrous HP (Fs) and the variable inconstant middle transition layer between the dense and serosal parts of the fibrous HP (M) were evaluated by identifying their distinct color boundaries from H&E and immunohistochemically stained samples (100x magnification). The total thickness of the HP without epipericardial adipose tissue = Fd + M + Fs, the total thickness of NAV = F + S + V. The relative thickness of the tissue layers as a percentage was calculated from layer thickness/total thickness. Fd/thk – the relative thickness (%) of the Fd layer of HP, F/thk – the relative thickness (%) of the F layer of NAV; M/thk – the relative thickness (%) of the M layer of HP, S/thk – the relative thickness (%) of the S layer of NAV, Fs/thk – the relative thickness (%) of the Fs layer of HP, V/thk – the relative thickness (%) of the V layer of NAV. The measurements were perfomed in the middle part of the NAV leaflet (the belly region) or in the HP samples from N = 3 NAV and N = 3 HP patients (tissue donors). Average values from 15 mesurements (n = 15) in each group of image files (NAV_F, NAV_S, NAV_V, HP_Fd, HP_M, HP_Fs) were used for a statistical evaluation.

### 2.6 Quantitative tissue analysis – ECM integrated density

A histomorphometric evaluation of the ECM structure was performed using ImageJ analysis software (Image Processing and Analysis in Java; National Institute of Health, USA) [13] from N = 3 NAV tissue donors and N = 3 HP tissue donors. Ten image files were scanned from each immunohistochemically-stained (collagen I, collagen III, elastin) or Alcian blue- stained (GAGs) sample, (100x magnification), giving a total of 30 images of HP and NAV. All images were acquired under identical conditions. The images have been digitized and stored in an uncompressed tagged image file format (image size 2088 × 1550 pixel) with 24-bit RGB. Ten lines of bar profiles were subsequently evaluated for each image sample for an investigation of the structure of the tissue. We evaluated this with the use of so-called ‘integrated density’ – the total amount of collagen I, elastin and mucopolysaccharides in the examined tissue was determined, with the exclusion of non-compacted tissue structures, which are artifacts resulting from the processing of histological samples. The content of investigated ECM proteins (collagen I, collagen III, elastin) and GAGs in the tissue was calculated as the integral of the density of the pixel values (color intensity) along the lines of the bar profiles (one slice intensity per row = ROI, n = 300 for each of the evaluated proteins and GAGs). This is like the tissue thickness of the stained ECM component multiplied by its color intensity [13–16].

### 2.7 An evaluation of biomechanical properties

#### 2.7.1 Uniaxial tensile testing

Uniaxial tensile tests were carried out with samples of HP and NAV, and the results were compared. The total number of tested samples was: 30 for HP from 12 patients (donors), and 10 for NAV from 5 patients (donors). The dimensions of the samples were contactlessly measured by laser-profiled ScanCONTROL 2800 (Micro – Epsilon, Ortenburg, Germany). Strips typically 0.2–0.5 mm in thickness, 3–5 mm in width, and 10–15 mm in length were prepared for mechanical testing. The NAV strips were cut in the longitudinal (circumferen- tial – NAV_L) or radial direction (NAV_R) of the NAV. The HP strips were cut transversely (HP_T) and longitudinally (HP_L) with respect to the orientation of the heart [Figure 1]. The number (n) of patients (donors) and the number of samples of the tested tissues is displayed in Table 1.

**Table 1.** Biomechanical properties. The number (*n*) of patients (donors) and samples of the tested tis- sues.

| Compared groups | Donors (n) | Samples (n) | b [mm] | h [mm] |
|---|---|---|---|---|
| HP_l | 12 | 20 | 5.05 ± 1.94 | 0.48 ± 0.17 |
| HP_t | 7 | 10 | 6.87 ± 1.25 | 0.64 ± 0.16 |
| naV_l | 5 | 5 | 4.07 ± 0.92 | 0.52 ± 0.19 |
| naV_r | 5 | 5 | 4.91 ± 0.64 | 0.49 ± 0.14 |

HP_l – human pericardium in the longitudinal direction; HP_t – human pericardium in the transversal direction; naV_l – normal (native) aortic valve in the longitudinal (circumferential) direction; naV_r – normal (native) aortic valve in the radial direction; b – width of the samples; h – thickness of the samples.

Mechanical experiments were performed on a tensile testing machine suitable for soft tissues (Messphysik Materials Testing GmbH, Fürstenfeld, Austria) equipped with a 25 N load cell. Deformations were assessed via image analysis of video records conducted by a built-in videoextensometer. Monotonic uniaxial loading was applied at a loading rate of 1 mm/s. This corresponds to strain rate dε/dt ≈ 0.1 s−1. The results were obtained after five cycles of preconditioning (loading/unloading), in order to attain repeatable behavior of a specimen. εmax was defined as the maximum strain (deformation) at which the stress increases monotonically (after this point, the slope to an σ–ε graph starts to decline, which indicates the initiation of a tissue failure process). Mechanical properties were evaluated from this last loading cycle. The evaluation of the mechanical properties was based on the secant elastic modulus Es, defined in (1).

$$E_s = \frac{\sigma_{\max}}{\varepsilon_{\max}} \tag{1}$$

Here, σmax is the maximum Cauchy stress achieved within the monotonic response of the material. It was computed as F·(1 + ε)/S; where F denotes loading force, S is reference cross-section area, and ε is engineering strain.

### 2.7.2 Ultimate tensile strength

UTS is the maximum stress that tissue samples can withstand while being stretched before breaking. UTS values were obtained from the stress-strain (σ–ε) curves for individual tissue samples. UTS was defined as a maximal value (the highest point) of Cauchy stress (σmax [MPa]) corresponding to the initiation of a tissue failure process at maximum (ultimate) tensile deformation (εmax [1]).

### 2.7.3 Flexural properties – bending stiffness

The tensile stress–strain curves (σ–ε) at low stress-low strain are related to the straightening of crimped fibres of collagen and the elongation of elastin fibers [18]. The bending stiffness (K) was estimated as the resistance of tissue samples to bending deformation for low stress- strain values (when the HP or NAV tissue was not damaged) according to the formula based on the Euler-Bernoulli equation [17,18]:

$$K = E_{0.02} I \quad \left[ Nm^2 \right] \tag{2}$$

where: $E_{0.02}$= mean elastic modulus value corresponding to low strain $\varepsilon$ = 0.02 [1], (2%); $I$ = second moment of inertia, calculated according to the formula:

$$I = \tfrac{1}{12} bh^3 \quad \left[ m^4 \right] \tag{3}$$

where: $b$ = width of the samples [mm]; $h$ = thickness of the samples [mm]. Rearranged for bending stiffness:

$$K = \frac{1}{12} b h^3 E_{0.02} \quad \left[ Nm^2 \right] \tag{4}$$

### 2.8 Statistical analysis

All parameters are expressed as means ± standard deviation, or as the median ± a range. A two-sample t-test or an unpaired Wilcoxon test for non-Gaussian distributed variables was used. All tests were two-sided, with $p < 0.05$ considered statistically significant. The statistical analyses were performed using MedCalc Software (Version12.1, Belgium).

The ECM histomorphometric data were evaluated using ANOVA and Student-Newman- Keuls multiple comparisons. The data were evaluated in the SigmaStat program (Systat Software, Inc., USA), and were expressed as the mean ± the standard error of the mean (SEM).

## 3. Results

### 3.1 Qualitative tissue analysis – a histological and immunohistochemical evaluation

#### 3.1.1 Comparison of HP and NAV tissue layers and the cellular structure

Normal HP consisted of three specific layers, (1) the inner layer of the serous pericardium facing the heart, (2) the fibrous part of the pericardium on the external side of the serous pericardium, which merges into (3) adipose tissue containing the neural elements and blood vessels surrounding the pericardium on the outer side [Figure 2]. The fibrous part of HP had no uniform structure, and was composed of three distinct layers – an outer dense part (Fd), an inner serosal (submesothelial) part adjacent to the parietal layer of serous pericardium (Fs), and a variable inconstant middle transitional layer between the dense and serosal parts of the fibrous HP (M). Comparing the HP with the NAV leaflets, H&E staining [Figure 2] delineated three distinct layers in the NAV: lamina fibrosa (F) on the outflow aspect, lamina spongiosa (S) in the middle, and lamina ventricularis (V) on the inflow aspect.

The surface parts of the HP and the NAV had different cellular structures [Figures 2, 3a and 3b]. Mesothelial cells with microvilli, which secrete the pericardial fluid that lubri- cates the surface of the pericardial cavity, formed a monolayer of flattened squamous-like epithelial cells. These cells were observed on the surface of the inner layer of the serous pericardium, and lined the pericardial sac. These cells rest on a thin basement membrane supported by dense connective tissue, and were stained positive for cytoskeletal proteins vimentin (a type III intermediate filament protein), α-SMA and β-catenin (a part of a pro- tein complex that creates adherens junctions that are important for maintaining epithelial cell tissue layers and barriers). However, the mesothelial cells were negative for the CD31 endothelial cell marker. Adipose tissue with capillaries composed of endothelial cells that stained positively for CD31 and beta-catenin was present on the outer side of the fibrous HP. The NAV leaflets were covered with valvular endothelial cells (VECs), which were positively stained for CD31 and β-catenin and negatively stained for vimentin and α-SMA. The ECM of the NAV is produced by VICs that exist in several phenotypes [Figures 2 and 3b]. VICs with a spindle-shaped (ellipsoidal) morphology due to the higher collagen I and III density of the ECM were present mostly in the lamina fibrosa. These cells were aligned along, and were in connection with, the stress-bearing collagen fibers. In the lamina spongiosa and lamina ventricularis, the VICs had a more spread-out polygonal morphology. Most VICs were positively stained for vimentin, a marker of cells of mesenchymal origin, characterizing a quiescent state of the VICs (qVICs). The NAV cusp tissue also contained a smaller number of α-SMA positive cells, which represented an activated myofibroblast-like VIC phenotype (aVICs). These cells were found predominantly in the lamina fibrosa of theNAV, and accounted for approximately 15% of all VICs.

The main cells in the fibrous part of HP were pericardial interstitial cells (PICs) [Figures 2 and 3a]. These cells are of mesenchymal origin and are capable of HP tissue remodeling, because, like VICs, they can produce and degrade ECM. PICs were found also in two phe- notypes – a quiescent fibroblast-like (qPICs) phenotype (displaying vimentin positivity) and an activated myofibroblast-like (aPICs)

phenotype (positively stained for α-SMA). As in the case of VICs, most of the PICs in the HP had a quiescent phenotype (qPICs). PICs and also VICs were desmin-negative and LCA-negative. In addition, no staining for β-catenin was evident between PICs and VICs. Ki-67 protein (also known as MKI67), which is strictly associated with cell proliferation, was found only sporadically and infrequently in the HP and NAV tissues. Only thinly dispersed individual PICs or VICs were Ki-67 positive. The cell shapes of both PICs and VICs corresponded to the structure of the surrounding ECM and the arrangement of its collagen fibers. The PICs in the dense part of the fibrous HP had a predominantly spindle-shaped (ellipsoidal) morphology, or less frequently a polygonal morphology, which was probably related to the higher collagen density of the surrounding ECM. However, the PICs in the serosal part of the fibrous HP had largely a spread-out polygonal morphology corresponding to the looser ECM structure.

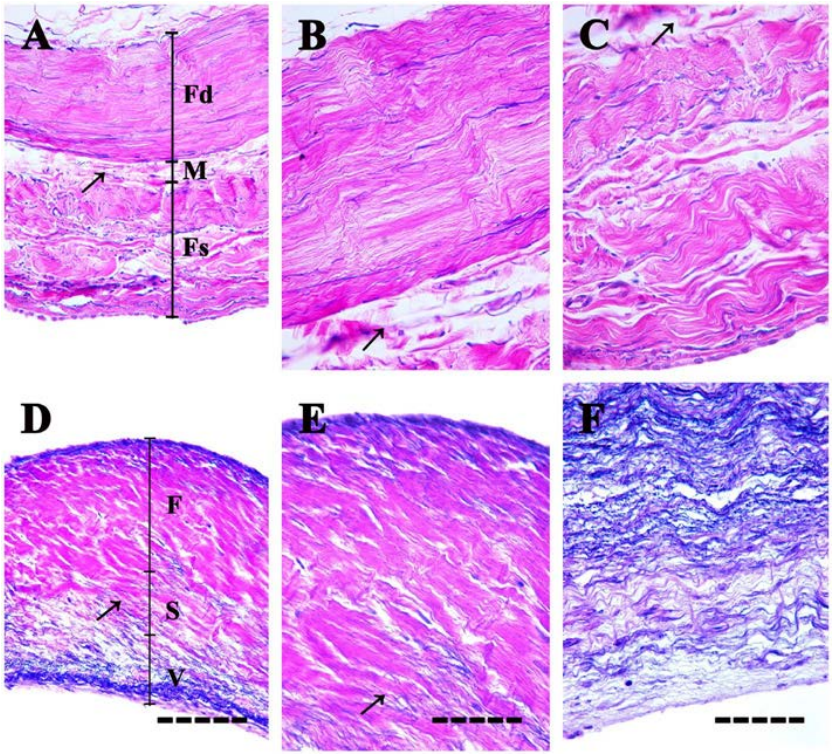


**Figure 2.** Hematoxylin-eosin and elastica Weigert – van Gieson staining (H&e) of HP (a, B, c) and naV (d, e, f). a, d – magnification 200x, scale bar = 200 μm, B, c, e, f – magnification 400x, scale bar = 100 μm. the nuclei of the cells are blue, the collagen fibers are red, the elastin fibers are blue-purple. HP: fd – outer dense part of fibrous HP (a, B), fs – the inner serosal (submesothelial) part of fibrous HP and the parietal layer of serous pericardium covered with mesothelial cells (a, c), and m – the inconstant variable middle transition layer between the dense and serosal parts of fibrous HP (a, B, c). naV: f – lamina fibrosa (d, e), s – lamina spongiosa (d, e, f) and V – lamina ventricularis (d, f). Notes: arrows in a,B,c - collagen and elastin fibers in the middle transition layer (m) connecting the dense and serosal parts of fibrous HP. arrow in d, e – collagen and elastin fibers in the middle layer, lamina spongiosa (s), connecting the lamina ventricularis and lamina fibrosa of naV.

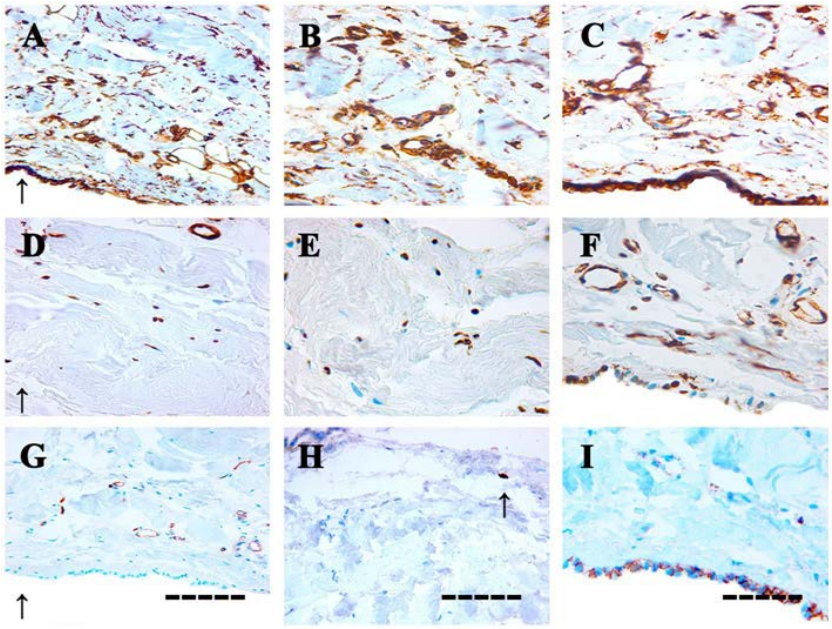


**Figure 3a.** cellular structure – immunohistochemical staining of HP. immunohistochemical staining for vimentin (a, B, c), α-sma, (d, e, f), cd31 (G), Ki-67 (H) and β-catenin (i), magnification 200x (a, d, G), scale bar = 200 μm, magnification 400x (B, c, e, f, H, i), scale bar = 100 μm. the immunopositivity of the targeted proteins in the cells is depicted in brown color, the nuclei are in blue. Notes: B, e, H - focused on the outer dense part of fibrous HP. c, f, i - focused on the inner serosal part of fibrous HP and the parietal layer of serous pericardium covered with mesothelial cells (arrows). Ki-67 proliferative marker positive staining was found only sporadically and infrequently in individual Pics in HP (H– arrow).

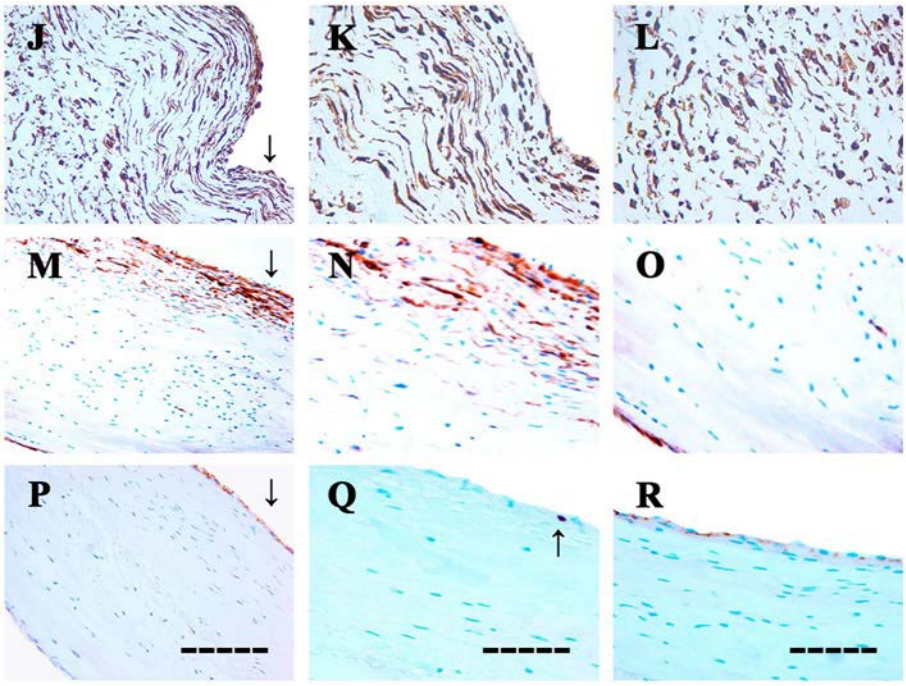


**Figure 3b.** cellular structure – immunohistochemical staining of naV. immunohistochemical staining for vimentin (J, K, l), α-sma, (m, n, o), cd31 (P), Ki-67 (Q) and β-catenin (r), magnification 200x (J, m, P), scale bar = 200 μm, magnification 400x (K, l, n, o, Q, r), scale bar = 100 μm. the immunopositivity of the targeted proteins in the cells is depicted in brown color, the nuclei are in blue.
Notes: arrows – lamina fibrosa, K, n, Q – focused on lamina fibrosa. l, o, r – focused on lamina ventricularis. Ki-67 proliferative marker positive staining was found only sporadically and infrequently in individual Vics in naV (Q – arrow).

### 3.1.2. A comparison between the polymeric structure of HP and NAV ECM

The ECM of HP and NAV had certain similarities in the composition of the polymeric pro- teins [Figures 2, 4a and 4b]. The ECM of the HP tissues and the NAV cusps was composed primarily of collagen type I, III, elastin and GAGs. Collagen I and III fibres represented the main stress-bearing polypeptides of both tissues.

The lamina fibrosa of the NAV consisted of rich collagen type I and III fibers that stained red on H&E [Figure 2]. These fibers were oriented parallel to each other, and displayed crimping with immunohistochemical staining [Figure 4b]. In the lamina fibrosa, the col- lagen fibres form a highly dense network of corrugated collagen fibers with a higher degree of alignment oriented preferentially in the circumferential (longitudinal) direction. In the lamina spongiosa and ventricularis of the NAV, collagen I and III fibres were present in smaller amounts than in the lamina fibrosa. They were more loosely packed and thinner. The lamina spongiosa also contained numerous transverse collagen I and collagen III fibers that connected the lamina fibrosa and lamina ventricularis into a bonded unit [Figures 2 and 4b]. The dense part of the fibrous HP consisted of thick, densely-packed fibers of collagen type I and III that had a characteristic crimped appearance on H&E, similar to that seen in the lamina fibrosa of the NAV. However, no alignment of the collagen fibres as in NAV was observed [Figures 2 and 4a]. A thin network of loosely arranged collagen fibers was seen in the variable middle transition layer between the dense and serosal parts of the fibrous HP. These collagen fibers were significantly less tightly packed than in the dense part of the fibrous HP, and resembled the collagen structure of the lamina spongiosa of NAV. However, transverse collagen I and III fibers connecting the tissue layers of fibrous HP were found in a significantly smaller amount in the variable middle transition layer between the dense and serosal parts of the fibrous HP [Figures 2 and 4a]. This was in contrast to their frequent occurrence in the lamina spongiosa of NAV. However, the inner serosal part of the fibrous HP, which theoretically corresponds to the inner lamina ventricularis of the NAV, had a significantly greater amount of collagen I and III fibers than the lamina ventricularis of the
NAV [Figures 2, 4a and 4b].

GAGs (glycosaminoglycans and proteoglycans) are very important for absorbing energy during compression in the cardiac cycle when NAV closes and opens. GAGs were found predominantly in the middle part of NAV, lamina spongiosa, where they formed a well-de- veloped and well-organized GAG tissue layer. GAGs were also distributed in other histo- logical layers of the NAV cusp, mainly in the

lamina ventricularis, but in a smaller amount than in the lamina spongiosa [Figure 4b]. GAGs were present uniformly in all layers of the fibrous HP, but in the inner serosal part they were observed in a larger amount than in the outer dense part [Figure 4a].

Elastin fibers (stained blue-purple on H&E) influence the elastic properties of the NAV tissue. They are thinner than collagen fibers and were observed among the wavily-arranged collagen fibers in all layers of the fibrous HP, which was similar to the arrangement seen in NAV [Figures 2, 4a and 4b]. However, there was an unequal distribution of elastin fibers between the two tissues. The organized network of elastin filaments that surround the collagen fibers bun- dles was present in smaller amounts in the NAV lamina fibrosa. The wavy elastin also formed connections between the collagen fibers and the elastin fibers of other NAV layers. Numerous wavily arranged elastin fibers were observed in the lamina spongiosa connecting the lamina ventricularis and the lamina fibrosa of NAV. Well-developed undulating and radially aligned elastin fibers were found predominantly in the lamina ventricularis of NAV, where they formed a characteristic dense sheet-like structure together with collagen I and III fibers. Overall, elastin fibres were observed in HP in smaller amounts in all layers than in NAV [Figures 2, 4a and 4b]. A denser concentration of elastin fibers was evident in the inner serosal part of the fibrous HP. In the HP, however, the elastin fibers were not arranged in such densely corrugated structures as were observed in the lamina ventricularis of NAV. In addition, the elastin fiber connections between the fibrous HP tissue layers were significantly smaller than in NAV.

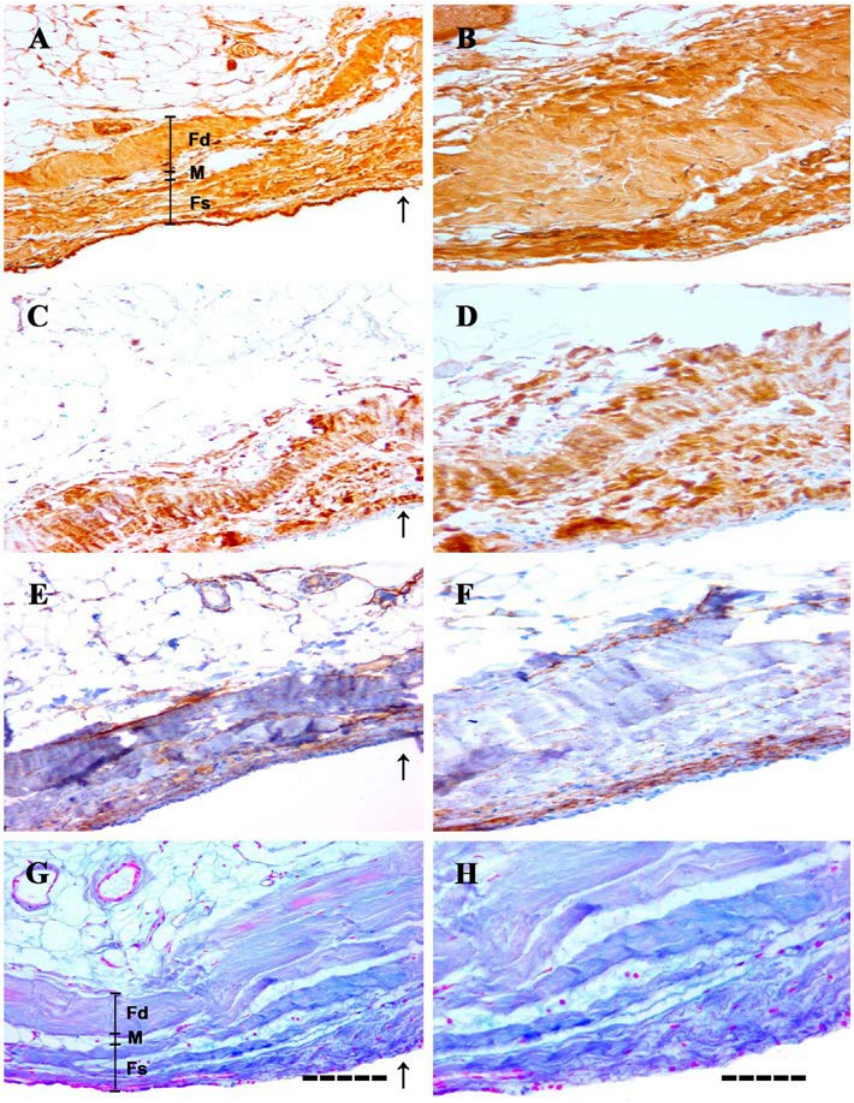


**Figure 4a.** ecm structure – immunohistochemical staining of HP. immunohistochemical staining for collagen type i (a, B), collagen type iii (c, d) and elastin (e, f); the samples are counterstained with Harris's hematoxylin. detected proteins are positive in brown color, nuclei are in blue. alcian blue staining for GaGs (G, H), positivity is shown in blue or dark blue, nuclei are in red. magnification 100x, scale bar = 400 µm (a, c, e, G), magnification 200x, scale bar = 200 µm (B, d, f, H). Notes: fd - outer dense part of fibrous HP, fs - the inner serosal (submesothelial) part of fibrous HP and the parietal layer of serous pericardium covered with mesothelial cells (arrows) and m - the inconstant variable middle transition layer between the dense and serosal parts of fibrous HP.

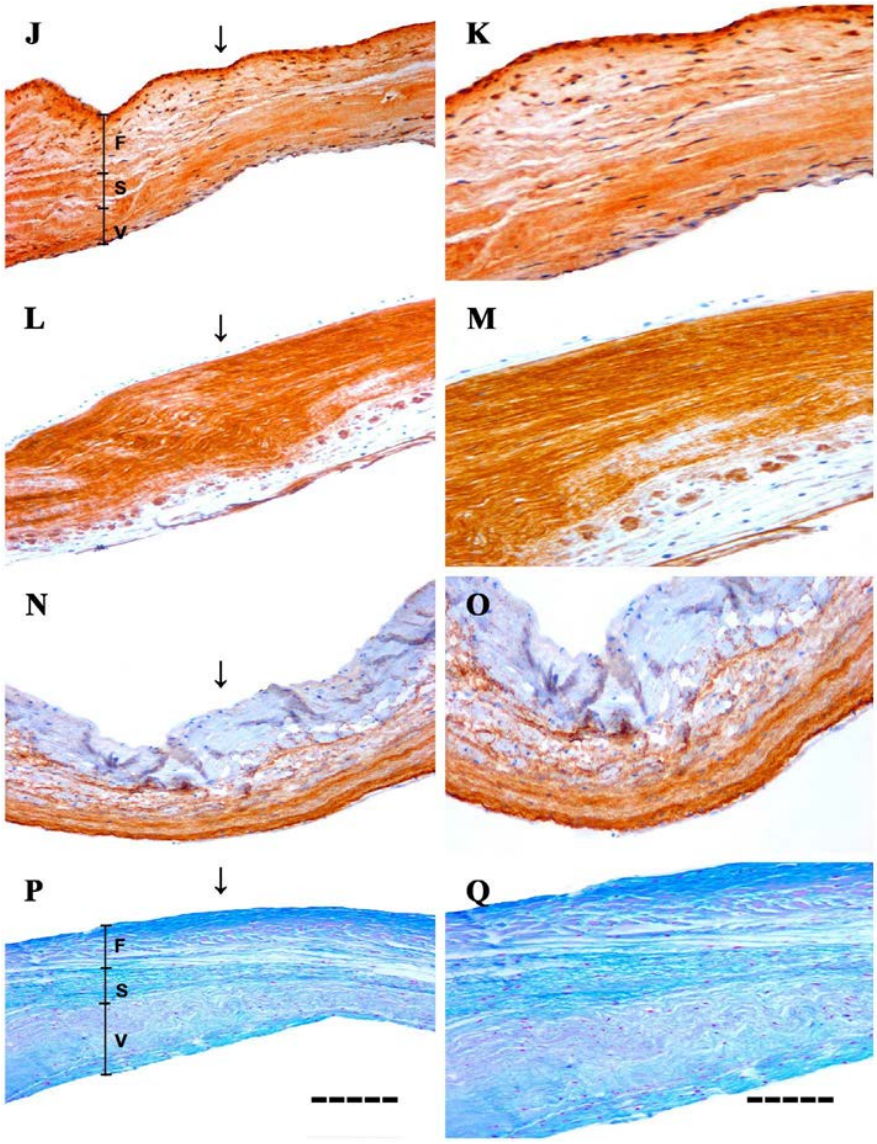


**Figure 4b.** ecm structure – immunohistochemical staining of naV immunohistochemical staining for collagen type i ( J, K), collagen type iii ( l, m) and elastin ( n, o); the samples are counterstained with Harris's hematoxylin. detected proteins are positive in brown color, nuclei are in blue. alcian blue staining for GaGs (P, Q), positivity is shown in blue or dark blue, nuclei are in red. Magnification 100x, scale bar = 400 µm ( J, l, n, P), magnification 200x, scale bar = 200 µm ( K, m, o, Q). Notes: f – lamina fibrosa (arrows), s – lamina spongiosa and V – lamina ventricularis. rich collagen i and iii fibers with crimping were present, mostly concentrated in the lamina fibrosa of the naV

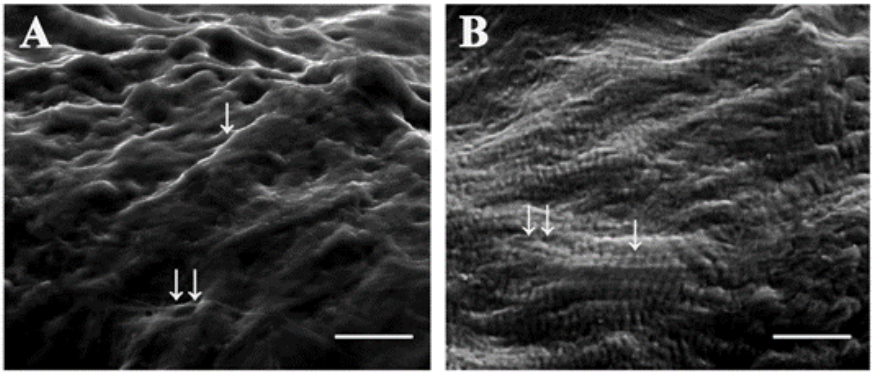


**Figure 5.** esem – surface morphology in relation to the arrangement of the collagen fibers. **(**a) – dense part of fibrous HP. (B) – lamina fibrosa of naV. scale bar = 50 µm. Notes: characteristic microscopis grooves and ridges (arrow) were observed on the surface of the dense outer part of the fibrous HP after removing the surrounding addipose tissue. A similar surface pattern (arrow) was observed on the outer surface of the lamina fibrosa of naV, covered by endothelial cells. Significant crimping and winding along the collagen bundles with corrugations was observed on the surfaces of both tissues. The branching and crossing of several thick collagen fiber bundles formed a multi-fiber knitted'tangle-like' pattern (two arrows).

### 3.2. ESEM – comparison of the surface morphology of HP and of NAV

ESEM of the HP and of the NAV cusp tissue (Figure 5) revealed close similarities in surface morphology related to the arrangement of the collagen fibers. When the adipose tissue was removed from the dense

outer part of the fibrous HP, we observed a typical homogeneous surface pattern with the use of ESEM. The outer surface of the pericardium (the dense part of the fibrous HP) and the lamina fibrosa (the ouflow part) of the NAV displayed characteristic microscopic grooves and ridges, which were formed by well-developed thick bundles composed of collagen fibers aligned in a highly parallel orientation.

Dense collagen fiber bundles arranged in the circumferential direction could play an important role in NAV leaflet coaptation. ESEM analysis showed the ridges of collagen bundles protruding beneath the NAV surface with great variability in their transverse radius, in the range from approximately 5–50 μm. Tree-like branching and crossing of several thick collagen fiber bundles on the NAV surface formed a multi-fiber knitted pattern. There was significant characteristic crimping and winding along the collagen fiber bundles. The corrugations were visible in the images as a regular alternation of dark and light bands, and corresponded to the alternating low and high-density collagen fibers. Thinner, multilayered collagen bundles with asymmetrical distribution and orientation, which overlapped each other, were also seen on the surface of the lamina fibrosa of NAV.

Characteristic surface corrugation patterns were also present on the surface of HP. Collagen fiber bundles were observed in the parallel direction, and mainly in the longitu- dinal direction. These ridges in the collagen bundles protruding beneath the surface of the HP were highly variable in their transverse radius, ranging between approximately 5–50 μm, as in the case of NAV. Thinner overlapping and multilayered collagen bundles were also observed, which had an asymmetrical distribution and orientation. Like the NAV surface, the HP surface had crimping and branching of the collagen bundles that formed a knitted architecture composed of several strands. However, the collagen fiber bundles were more loosely arranged and more unwound in the HP than in the NAV.

### 3.3. Second harmonic generation (SHG) and two-photon excitation microscopy (TPEM)

#### 3.3.1. A comparison of the architecture of HP and NAV collagen and elastin fibers

The surface layers of the HP and NAV tissues and the arrangement of the collagen and elastin fibers in fresh and unfixed specimens were better shown by SHG and TPEM microscopy [Figures 6a and 6b]. There were multilayered, multidirectionally oriented and overlapping collagen fiber bundles (the magenta SHG signal) forming a densely woven network in HP. The fibers tended to be oriented longitudinally in relation to the HP harvested from the anterior part of the heart [see Figure 1]. Branching collagen fibers crossing the collagen bundles perpendicularly and connecting other collagen bundle layers were also observed. This arrangement of collagen fibers may be important for the integrity of the HP tissue, and for its biomechanical properties. More homogeneous, thicker, dense and multilayered collagen fiber bundles were observed in the dense part than in the serosal part of the fibrous HP. The collagen fibers were also more highly aligned and arranged in a parallel direction in the dense part of the fibrous HP. In the inner serosal part of the fibrous HP, the collagen formed multilayered fiber bands, which overlapped each other in various directions, and were thinner and more loosely arranged than in the dense part of the fibrous HP. The col- lagen fibers had a characteristic sinusoidal pattern with a crimped period of approximately 10–35 μm and an amplitude of 3–12 μm in both parts of the fibrous HP.

The NAV cusps displayed a well-developed crimped and densely-packed network of col- lagen fibers. The density of the parallel collagen fibers was highest on the side of the lamina fibrosa of the NAV. In the lamina ventricularis of the NAV, the collagen fibers were more loosely packed in a non-uniform direction. They were more disordered and were tangled. The collagen fibers in the lamina fibrosa and lamina ventricularis of the NAV also had an expressed common sinusoidal pattern, but with a shorter crimped period of approximately 4–19 μm and a lower amplitude of 2–3 μm in comparison with the fibrous HP.

The elastin fibers (bright green SHG autofluorescence) were much thinner than the collagen fibers, and formed a branched network around the collagen fibers and cells. They were well developed in the lamina fibrosa of the NAV, where they were arranged both in the parallel direction and in the longitudinal

direction with respect to the col- lagen fibers. The elastin fibers in the lamina ventricularis of the NAV were denser than in the lamina fibrosa, and formed a more complex dense sheath-like structure. The elastin fibers were also more wavily arranged in the lamina ventricularis than in the lamina fibrosa of NAV. This arrangement of elastin fibers is responsible for the elastic recoil during NAV closure.

Elastin fibers occurred only rarely, and were present in smaller amounts in the HP tissue than in the NAV. In the dense part, the elastin fibers were loosely arranged and they were present in smaller amounts than in the serosal part of the fibrous HP. There were particularly well developed elastin fibers, which were wavily arranged and formed a network that was related to the main direction of the collagen fibers.

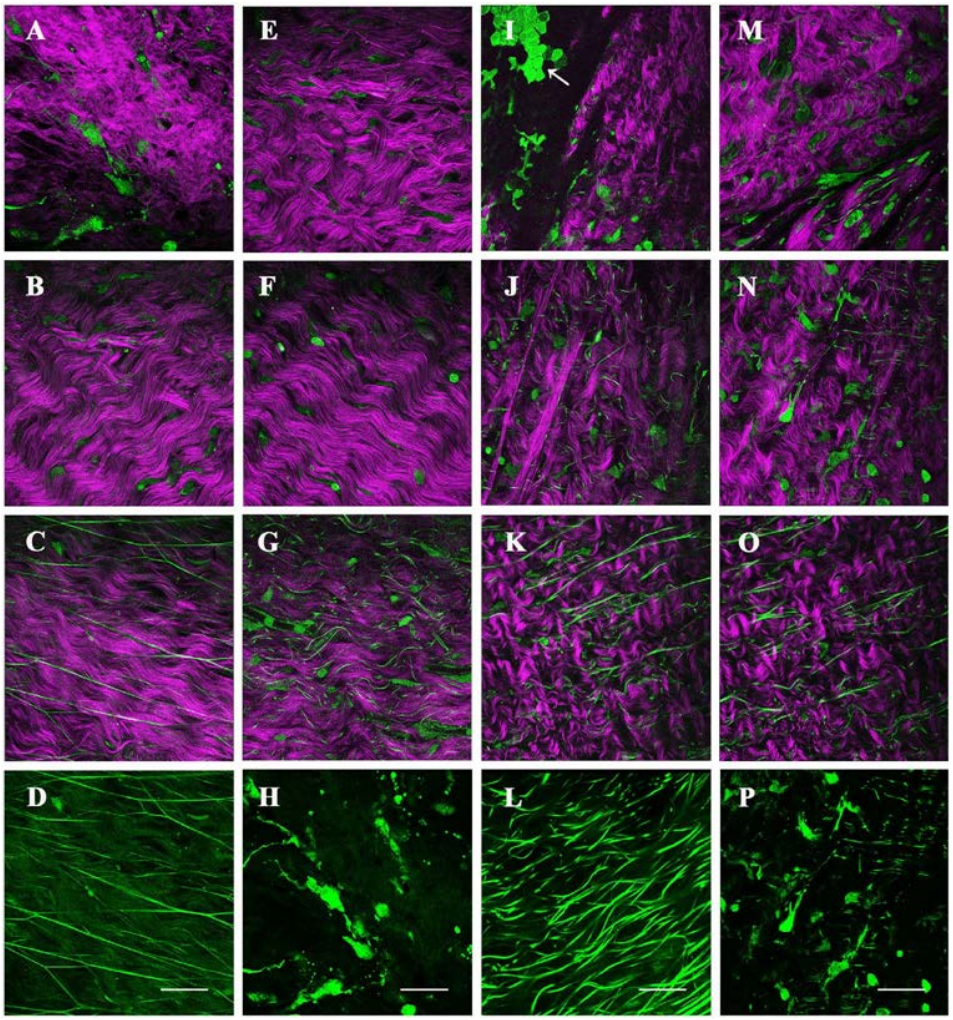


**Figure 6a.** second harmonic generation (sHG) and two-photon excitation microscopy imaging (tPem) of HP. Bright green fluorescence – 5 chloromethylfluorescein diacetate (cmfda) staining of living cells (Pics and mesothelial cells) and autofluorescence of elastin, magenta – sHG signal of collagen. a – H = outer dense part of fibrous HP, i – P = inner serosal part of fibrous HP. d, H, l, P – focused on the arrangement of the elastin fibers and the living cells (Pics). Scale bar = 50 μm. Notes: Pics connections and interactions with ecm were observed in the tissue layers of HP. the surface of the inner serosal part of HP (facing the heart) was covered by squamous flattened mesothelial cells with microvilli (i arrow).

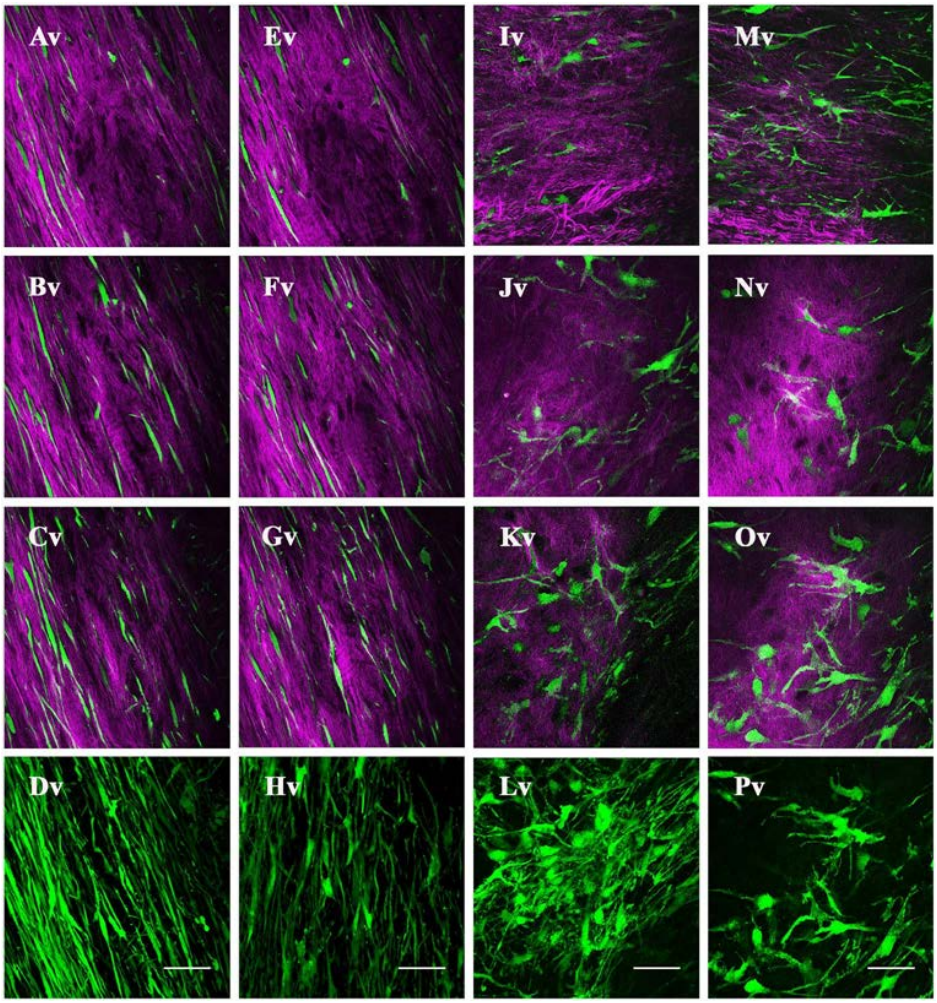


**Figure 6b.** second harmonic generation (sHG) and two-photon excitation microscopy imaging (tPem) of naV. Bright green fluorescence – 5-chloromethylfluorescein diacetate (cmfda) staining of living cells (Vics) and autofluorescence of elastin, magenta – sHG signal of collagen. av – Hv= lamina fibrosa, iv – Pv = lamina ventricularis. dv, Hv, lv, Pv – focused on the arrangement of the elastin fibers and the living cells (Vics). Scale bar = 50 μm. Notes: Vics connections and interactions with ecm were observed in the tissue layers of naV.

### 3.3.2. The shape of live PICs and VICs, and cell-ECM interactions

Live PICs and VICs exhibited an intensely green florescence and well-developed cyto- plasmic processes (filopodia) when stained with CMFDA [Figures 6a and 6b]. In both HP and NAV, the frequency and the shape of the live PICs and VICs corresponded to the arrangement of the surrounding ECM, and was mainly related to the density of the collagen fibers. Live VICs in the lamina fibrosa were predominantly spindle-shaped (ellipsoidal), and were oriented along the circumferentially-aligned densely-packed collagen fibers. This unique spindle cell morphology accommodated the collagen fiber structure. Similarly, live PICs in the dense part of the fibrous HP had a predominantly spindle-shaped (ellipsoidal) morphology. Less frequently, they had a polygonal morphology. Live PICs in the serosal part of the fibrous HP frequently had a characteristic spread-out polygonal morphology, similar to the morphology displayed by live VICs in the lamina ventricularis of the NAV with more loosely-arranged collagen fibers.

The VICs cellular processes (filopodia) were aligned in parallel to the collagen fibers that the cells produce and remodel in relation to the deformation forces.These filipodia were also visible in the PICs in the HP tissue. They formed connections and formed a complex three-dimensional network between the cells and between the collagen and the elastin fib- ers. Points of cellular attachment of VICs and PICs to the collagen and elastin fibers were observed. However, they were present to a lesser extent in the HP than in the NAV. These connections could be important for the transfer of external mechanical stimuli from the ECM polymeric components to the cells.

## 3.4. Quantitative tissue analysis – histomorphometry

### 3.4.1. Stratification of HP and NAV tissue layers

A histomorphometric evaluation was used to compare the overall thickness of the HP and the NAV, and the relative thickness of individual layers of both tissues [Table 2]. Although the average total thickness of the HP was greater than that of the NAV, the differences between the two tissues were not statistically significant. The relative thickness of the dense part of the fibrous HP (Fd) was 49 ± 2%, which was similar to the relative thickness of the main load-bearing structure of the NAV, lamina fibrosa (F) 47 ± 4%. However, our results showed that the proportions of the other tissue layers of the HP and the NAV differed sig- nificantly. The relative thickness of the variable and inconstantly present middle transition layer between the dense parts and the serosal parts of the fibrous HP (M) was significantly smaller ($p < 0.001$) than the middle part of the NAV, the lamina spongiosa (S) (4 ± 4% and 29 ± 4%, respectively). Also, the relative thickness of the serosal part of the fibrous HP (Fs) (47 ± 2%) was almost twice that of the lamina ventricularis (V) of the NAV (24 ± 3%). These differences were statistically significant ($p < 0.001$).

**Table 2.** HP and naV tissue layers stratification by histomorphometry.

| Tissues/layers | thk (µm) | Fd ≈ F (µm) | M ≈ S (µm) | Fs ≈ V (µm) | Fd ≈ F /thk (%) | M ≈ S /thk (%) | Fs ≈ V /thk (%) |
|---|---|---|---|---|---|---|---|
| HP (*n* = 15) | 574 ± 112 | 280 ± 52 | 26 ± 23 | 268 ± 48 | 49 ± 2 | 4 ± 4 | 47 ± 2 |
| naV ( *n* = 15) | 565 ± 60 | 264 ± 27 | 167 ± 31 | 134 ± 27 | 47 ± 4 | 29 ± 4 | 24 ± 3 |
| *p* value | 0.73 (ns) | 0.25 (ns) | *p* < 0.001* | *p* < 0.001* | 0.08 (ns) | *p* < 0.001* | *p* < 0.001* |

notes: *n* = number of evaluated tissue samples; HP – human pericardium; naV – normal (native) aortic heart valve; thk – total thickness of the tissue samples; fd – dense part of fibrous HP; f – lamina fibrosa of naV; m – inconstant middle transition layer between the dense and serosal (submesothelial) parts of fibrous HP; s – lamina spongiosa, middle part of naV; fs – serosal (submesothelial) part of fibrous HP; V – lamina ventricularis, inner part of naV. total thickness of HP without epipericardial adipose tissue = fd + m + fs, total thickness of naV = f + s + V. fd/thk – relative thickness (%) of the fd layer of HP, f/thk – relative thickness (%) of the f layer of naV; m/thk – relative thickness (%) of the m layer of HP, s/thk – relative thickness (%) of the s layer of naV, fs/thk – relative thickness (%) of the fs layer of HP, V/thk – relative thickness (%) of the V layer of naV. an asterisk indicates a group with significant differences. the differences in the total thickness and in the relative thickness of fd ≈ f layers between HP and naV were not statistically significant. a two-sample t-test revealed significant differences (*p-value* < 0.001) in m ≈ s and fs ≈ V layer thickness between HP and naV.

### 3.4.2. ECM integrated density

The biopolymeric composition of HP and NAV was evaluated by histomorphometric anal- ysis of ECM integrated density [see Figure 7]. HP contained a greater amount of collagen I and a lower amount of collagen III and elastin than NAV, and a similar amount of GAGs, as measured by the integrated pixel values (color density), corresponding to the total amount of proteins and GAGs in the tissue. There were statistically significant differences between HP and NAV with respect to collagen I, collagen III and elastin content ($p < 0.001$), but the differences were not significant for the GAGs content.

Collagen I and III were the main load-bearing proteins of the HP and NAV tissues. The differences in collagen I content were related to the denser arrangement of its fibers in the serosal part of the fibrous HP, rather than to their relatively sparse occurence in the cor- responding lamina ventricularis of NAV. The higher collagen III content in the NAV than in the HP was caused by the presence of more densely packed collagen III fibers in the lamina fibrosa and spongiosa of NAV than in the dense or serosal part of the fibrous HP. The lower elastin content in the HP than in the NAV was in relation to the different elastin fiber architecture in both tissues. Although a non-uniform distribution of GAGs in the HP and NAV histological layers was observed, there was no difference in the total GAGs content in the two tissues.

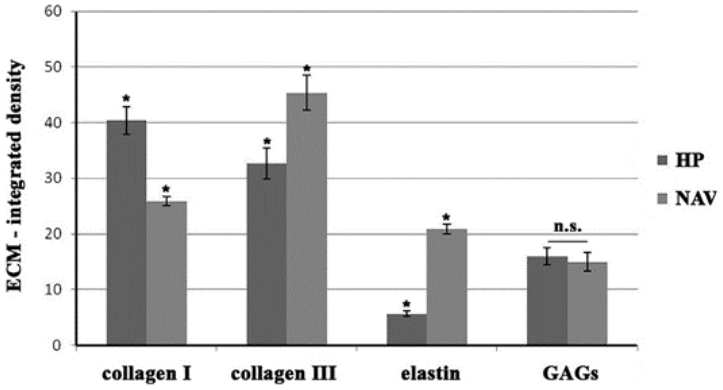


**Figure 7.** Quantitative tissue analysis – ecm integrated density. Notes: Histomorphometric analysis was performed using the imageJ analysis program (image Processing and analysis in Java; national institute of Health, usa) in each group of HP and naV. the content of investigated ecm polymeric proteins calculated as the integral of the density of the pixel values (color intensity) along the lines of the bar profiles (n) was measured from immunohistochemical staining images for collagen i ($n$ = 300), collagen iii ($n$ = 300), elastin ($n$ = 300) and GaGs ($n$ = 300). ecm of HP showed that there was a larger amount of collagen i, but a smaller amount of collagen iii and elastin than in naV. the differences between the groups were statistically significant: *$p$ < 0.001. no statistically significant differences between the two tissues were found for the ecm GaGs content. the data are presented as mean ± sem.

## 3.5. An evaluation of the biomechanical properties of HP and NAV

### 3.5.1. Uniaxial tensile testing

We compared the mechanical properties of the two tissue samples in the same directions, i.e. we compared HP_L with NAV_L, and HP_T with NAV_R. The HP_T samples were of greater thickness and width than the HP_L or NAV_R samples. Otherwise there was no significant difference in laser-based measured thickness (thk) between the HP and NAV tis- sues. The stress-strain (σ–ε graphs) relationships for the evaluated tissue samples are shown in Figure 8. Mechanical experiments determined the secant elastic moduli for the tested tissue specimens, as follows: HP_L – Es = 39.91 ± 27.59 MPa, HP_T – Es = 15.56 ± 7.24 MPa, NAV_L – Es = 30.84 ± 11.69 MPa, NAV_R – Es = 14.28 ± 6.54 MPa [Table 3]. The Es values were greater for both tissues in the longitudinal direction, and a two-sample t-test revealed significant differences ($p < 0.05$) in Es between HP_L and HP_T, and between NAV_L and NAV_R. However, a two-sample t-test revealed no significant differences in Es between HP_L and NAV_L, and between HP_T and NAV_R [Table 4].

### 3.5.2. Ultimate tensile strength (UTS)

The results for maximum tensile strains (εmax [1]) and for the corresponding UTS [MPa] in the compared groups are displayed in Table 3. The maximum εmax [1] levels were greater for HP_T than for HP_L ($p < 0.05$), and were greater for NAV_R than for NAV_L. This was in relation to the width and thickness of the samples. The UTS values for both tissues were higher in the longitunal direction than in the transversal or radial directions. However, a two-sample t-test revealed no significant differences in UTS between HP_L and NAV_L, and between HP_T and NAV_R [Table 4].

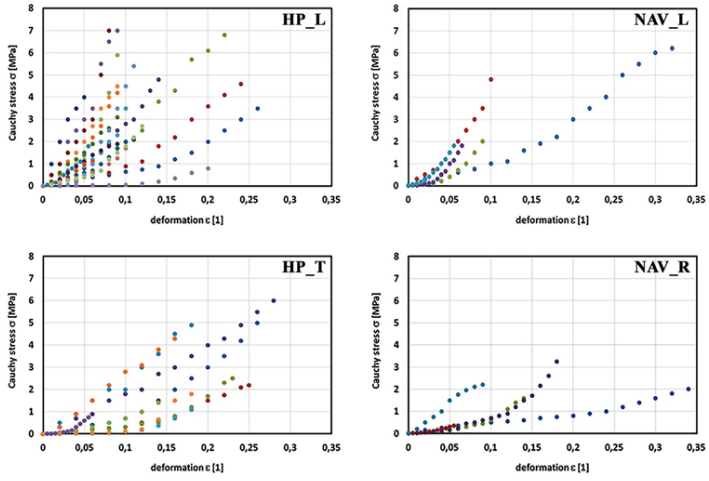


**Figure 8.** evaluation of biomechanical properties – cauchy stress ($\sigma$) and strain ($\varepsilon$) relationship graphs for evaluated tissue samples. Notes: x axis of the graphs – deformation (strain) $\varepsilon$ [1]; y axis of the graphs – cauchy stress ($\sigma$) in [mPa]; HP_l – human pericardium in the longitudinal direction; HP_t – human pericardium in the transversal direction; naV_l – normal (native) aortic heart valve in the longitudinal (circumferential) direction; naV_r – normal (native) aortic heart valve in the radial direction. uts is the highest point of the cauchy stress ($\sigma$max – [mPa]) corresponding to the initiation of a tissue failure process at maximum (ultimate) tensile deformation ($\varepsilon$max[1]).

**Table 3.** Biomechanical properties.

| Compared groups | Es [MPa] | εmax [1] | UTS [MPa] | E0.02 [kPa] | *K* [k N.m2 ] |
|---|---|---|---|---|---|
| HP l | 39.91 ± 27.59 | 0.12 ± 0.06 | 4.11 ± 2.54 | 798.20 ± 551.91 | 32.8 ± 28.9 |
| HP t | 15.56 ± 7.24 | 0.19 ± 0.07 | 2.99 ± 1.88 | 311.20 ± 144.89 | 54.4 ± 37.7 |
| naV l | 30.84 ± 11.69 | 0.13 ± 0.11 | 3.36 ± 2.02 | 616.80 ± 233.90 | 35.8 ± 42.1 |
| naV_r | 14.28 ± 6.54 | 0.17 ± 0.12 | 1.92 ± 1.06 | 285.60 ± 130.85 | 16.9 ± 14.4 |

Notes: HP_l – human pericardium in the longitudinal direction; HP_t – human pericardium in the transversal direction; naV_l – normal (native) aortic heart valve in the longitudinal (circumferential) direction; naV_r – normal (native) aor- tic heart valve in the radial direction; es – secant elastic modulus; strain εmax – strain at ultimate tensile stress; uts – ul- timate tensile strength; e0.02= mean elastic modulus value corresponding to a low strain ε = 0.02 [1], (2%); *K* – bending stiffness.

**Table 4.** Results of a two-sample t-test and the corresponding *p-values* in the compared groups.

| Compared groups | b *p-value* | h *p-value* | Es *p-value* | εmax *p-value* | UTS *p-value* | E 0.02 *p-value* | *K* *p-value* |
|---|---|---|---|---|---|---|---|
| HP l – HP t | **0.0124*** | **0.0274*** | **0.0098*** | **0.0078*** | 0.2314 | **0.0110*** | 0.0927 |
| naV l – naV r | 0.1619 | 0.8382 | **0.0245*** | 0.2108 | 0.2885 | **0.0484*** | 0.3531 |
| HP l – naV l | 0.2890 | 0.7108 | 0.4508 | 0.8951 | 0.5487 | 0.4849 | 0.8485 |
| HP_t – naV_r | **0.0063*** | 0.1207 | 0.7450 | 0.5844 | 0.2616 | 0.7451 | 0.0545 |

Notes: HP_l – human pericardium in the longitudinal direction; HP_t – human pericardium in the transversal direction; naV_l – normal (native) aortic heart valve in the longitudinal (circumferential) direction; naV_r – normal (native) aor- tic heart valve in the radial direction; b – width of the samples; h – thickness of the samples; es – secant elastic modulus; strain εmax – strain at ultimate tensile stress; uts – ultimate tensile strength; e0.02＝mean elastic modulus value corre- sponding to a low strain ε = 0.02 [1], (2%); *K* – bending stiffness. an asterisk indicates a group with significant differences (*p-value* < 0.05).

### 3.5.3. Flexural properties – bending stiffness

The results of E0.02, the mean elastic modulus value corresponding to a low strain ε = 0.02 [1], (2%) and bending stiffness (K) in the compared groups, are displayed in Table 3. The E0.02 values were greater for both tissues in the longitudinal direction ($p < 0.05$). The cal- culated bending stiffness values were greater for HP_T than for HP_L and were greater for NAV_L than for NAV_R. The greater bending stiffness values for HP_T than for HP_L may be related to the dimensions of the samples. However, no statistically significant differences in the calculated bending stiffness were found between the two tissues in the longitudinal direction and in the transversal or radial directions [Table 4].

## 4. Discussion

Since there are currently no acceptable autologous scaffolds for heart valve tissue engineer- ing, we performed a study aimed at comparing the ECM biopolymeric structure and the biomechanical properties of the HP and human NAV. We have found several important similarities between the two tissues. HP and human NAV contain cells of mesenchymal origin (PICs and VICs, respectively), which are specifically arranged in the ECM structure and exist in several phenotypes – embryonic progenitor endothelial/mesenchymal cells, quiescent VICs (qVICs), activated VICs (aVICs), progenitor VICs (pVICs), and osteo- blastic VICs (obVICs) [19]. Like the VICs in NAV, the PICs in the fibrous HP exist in a quiescent (fibroblast-like) and activated (myofibroblast-like) phenotype [19,20]. Like VICs, most PICs exist in a quiescent (fibroblast-like) phenotype. PICs are able to respond to the mechanical stresses in vitro by proliferating and differentiating into an activated phenotype (aPICs). Activated PICs can produce and remodel ECM [21]. Ki-67 is a nuclear protein that is associated with, and may be necessary for, cellular proliferation (RNA transcipriton) [22]. During mitosis, most of the protein is relocated to the surface of the chromosomes. This protein is absent in resting cells. For example, Ki-67 is physiologically present in the basal layer of the skin and in the epithelial cells of the gastrointestinal tract. It is also patho- logically increased in actively growing tumors, especially in malignant tumors [22,23]. In native HP, as in human NAV, Ki-67 was found only sporadically and infrequently. Cell-to-cell and cell-to-surrounding ECM communications were well visible by SHG microscopy and by TPEM in both HP and NAV tissues [see Figures 6a and 6b]. These cells interact not only with the ECM, but

also with each other through cytoplasmatic extensions and cellular junctions. This confirms the existence of a complex three-dimensional PICs and ECM network very similar to that of the NAV, with intimate associations present between cells, and between cells and collagen and elastin fibers. Several molecules are involved in these communications; N-cadherin (cadherens junction), desmoglein (desmosomal junction), connexins 26 and 45 (gap junction), integrin molecules α1, α2, α3, α4, α5, α6 and β1 [24]. This three-dimensional connecting network and these cell associations are important for sensing strains and stresses in valve tissue, and for reacting to them appropriately. It was confirmed in vivo that the cellular response to mechanical stimulation can be influenced by the direction of the applied forces, by the ECM architecture, and by the cell morphology and orientation [25,26]. Forces exerted on the ECM by the flow of blood in vivo are sensed by VICs through cell-ECM adhesions [26]. As has been documented by SHG/TPEM imaging in our study, the shape of the VICs and also of the PICs is related to the surrounding ECM structure, specifically to the arrangement of the collagen fibers. The collagen fiber micro- structure is organized to induce consistent VICs and PICs deformation in vivo. VICs in the lamina fibrosa of the NAV are under the greatest oscillatory shear stress, tensile stretch and pressure forces [27]. Increased mechanical strain within the valve tissue correlates with elongation of the nuclear and cellular shape of VICs [18]. VICs with a spindle-shaped morphology in the collagen-rich fibrosa layer are significantly more deformed at diastolic pressures than VICs with a spread-out polygonal morphology in the spongiosa-ventricular layer, which are less deformed because of a lack of compacted collagen fibers [28,29]. We can assume that there is a similar relationship between stress-strain loading and the shape of the PICs and the ECM structure in HP tissue.

Mechanical signals are detected intracellularly by signal transduction pathways, which influence the function and the genetic behavior of cells [26]. VICs continuously respond to their environment by proliferating and differentiating to an activated myofibroblast-like contractile phenotype called aVICs (with gene ACTA2 expression) [29]. aVICs produce, remodel and crosslink the ECM through the production of several enzymes, such as lysyl oxidase (LOX), lysyl hydroxylase, matrix metalloproteinases (MMPs – collagenase-1, colla- genase-3) and their inhibitors (TIMPs) [3,28]. Natural collagen crosslinking within the ECM is influenced by the biological environment, and depends on the amino acid sequences and the specific quaternary structural arrangements of the collagen [30]. The unique biological behavior of VICs permits heart valve tissue growth, and also repair and adaptation on cir- culatory forces [26]. This is important for maintaining long-term heart valve integrity and function. The amount and the quality of the ECM that is produced, e.g. the orientation of the collagen fibers, the collagen type and the degree of crosslinking determine the mechanical properties of the tissue, including compliance, elastic modulus and tensile strength [18]. This cellular behavior and continuous repair and remodeling is especially important for connec- tive tissue that serves as a structural scaffold for load bearing, such as the heart valve [26]. The surface of NAV is covered by endothelial cells (VECs), which have site-specific mechanical properties and play an important role in protection against calcific disease by preventing the differentiation of VICs into pathological cell phenotypes and by regulating the ECM structure of the valve [31,32]. However, mesothelial cells that cover the surface of serous HP do not have the structure or the function of VECs. The main function of meso- thelial cells is to produce a lubricating fluid that is released into the pericardial cavity [8]. Mesothelium derives from the embryonic mesoderm cell layer that lines the coelom (body cavity) in the embryo and develops into the layer of cells that covers and protects most of the internal organs of the body [33,34]. The mesodermal origin of these epithelial layer cells is the reason why they are positively stained for vimentin and α-SMA [33,34]. In vitro, or after implantation of an autologous pericardial heart valve replacement in vivo, the surface of the HP valve replacement may be endothelialized and become covered by the patient’s own endocardial and endothelial cells (originating from circulating endothelial progenitor cells). This can be due to the presence of specific amino acid sequences and other ligands for cellular adhesion receptors on the surface of the pericardial ECM, which is considered to be an attractive substrate for the adhesion of endothelial cells [35,36]. Such endothelization was also observed after the implantation of off-the-shelf human decellularized TEHVs in a non-human primate model [37].

ESEM technology [38] makes it possible to investigate specimens in their natural state under the conditions of a water vapour atmosphere in a microscope chamber with pressures adjustable up to 2600 Pa (=26 mbar = 20 Torr). Gas (water vapor) ionization inhibits the accumulation of a charge on the

surface of non-conductive specimens, and amplifies the secondary electron signal. This technology does not require time-consuming conventional preparation techniques (such as desiccating and gold-palladium vacuum coating), which may produce unwanted artifacts in the sample. In addition, the cooling system enables easily-damaged living specimens to be examined by freezing them to temperatures between 0 °C and −20 °C with 0.1 °C accuracy. Cooling is effective in reducing the adverse effects of over-drying, which could cause the samples to become wizened. Cooling is also effective in preventing the burns or swellings that are made by an intensive electron beam. Together with high resolution (up to 3.5 nm at 30 kV) electron optics and a sensitive GSED, this provides the ability to observe the natural state of biological specimens under magnification from 6x up to 20,000–50,000x, depending on the quality of the sample material (the maximum magnification of the microscope is >1,000,000x).

ESEM of the HP and NAV cusp tissue revealed close similarities in surface morphology related to the architecture of the collagen fiber bundles. The outer surface of fibrous HP displayed microscopic grooves and ridges formed by well-developed thick collagen fiber bundles, which resemble those of the lamina fibrosa of NAV. This specific surface pattern with corrugations corresponded to low and high density of the collagen fibers. The colla- gen bundle ridges protruding beneath the HP and NAV surfaces were very variable, but their transverse radii had similar values. However, the collagen bundles were more loosely arranged and more unwound in HP than in NAV. Non-uniform and bent collagen bundles were observed that angled downward from the commisures toward the center of the NAV leaflets, with the highest collagen fiber density and bundles larger in diameter in the middle part (belly area) of the cusps, and smaller when they are closer to the free edge or to the low point of the fixed end [39]. A correlation between the orientation angle of the local collagen fibers and the local stress distributions was confirmed. The global average angle of the collagen fibers oriented in the circumferential direction was measured as 36–59º in porcine aortic heart valve cusps. This is probably not different from the average angle for human NAV [40]. The corresponding predominant orientation of the collagen fibers in the HP from the anterior part of the heart tends to be in the longitudinal direction with respect to the orientation of the heart.

In our study, we compared the histological stratification and the ECM composition of the HP and NAV tissue layers. Although the differences in the total thickness of the tissue samples between HP and NAV were not statistically significant, we observed differences in the relative proportions of particular tissue layers between HP and NAV. The relative thickness of the dense part of the fibrous HP (Fd) (49 ± 2%) was similar to the relative thickness of the main load-bearing layer of the NAV, lamina fibrosa (F). However, the proportions of the other tissue layers of the HP and the NAV were significantly different. The relative thickness of the variable middle transition layer that was present between the dense and serosal parts of the fibrous HP (M) was significantly less ($p < 0.001$) than the corresponding middle lamina spongiosa of the NAV, and contained only loosely arranged collagen I and III fibers. The relative thickness of the serosal part of fibrous HP (Fs) was conversely significantly ($p < 0.001$) thicker than the lamina ventricularis (V) of the NAV, due to the presence of more densely arranged collagen I and III fibers.

NAV leaflets are composed primarily of collagen (60% of the total dry weight of ECM). The most abundant types of collagen in the NAV are collagen I (74% of the total collagen) and collagen III (24% of the total collagen) [41,42]. Fibrillar collagens consist of 3 coiled polypeptide chains that are tightly packed in a parallel arrangement, forming a triple α helix. Collagen type I is a heterotrimer of α1 and α2 chains, while collagen type III is a homo- trimer of α1 chains [43]. The coils are about 300 nm long, and are connected together in a staggered D-banding pattern with a periodicity of 67 nm [44]. These collagen microfibrils (procollagen) are crosslinked into the ECM and are arranged into fibrils (tropocollagen), which are packed together in the fibrillogenesis process to form fibers (bundles of fibrils) [43]. Collagen fibers, which are the main load-bearing component of NAV, are oriented predominantly in the direction of the largest tensile stress [26].

SHG and TPEM enabled us to compare the nature and the arrangement of the collagen fibers in fresh and unfixed HP and NAV tissue specimens. Some differences were found between the HP and NAV

tissue layers. In the dense part of the fibrous HP, collagen fib- ers formed thick, dense, multilayered and highly aligned bundles arranged in the parallel direction. The characteristic arrangement of the collagen fibers in this part of the fibrous HP resembled the highly aligned dense collagen fiber network of the lamina fibrosa of the NAV. However, in the lamina fibrosa of NAV the density and the alignment of the collagen fibers were higher than in HP. The collagen fibers in the inner serosal part of fibrous HP were more loosely arranged and thinner than the dense part of fibrous HP. This could be because the inner serosal part of fibrous HP is exposed to lower stretching and stress under physiological conditions than the dense outer part of it. However, collagen I and collagen III fibers were found more frequently in the serosal part of the fibrous HP, and they were thicker than in the inner lamina ventricularis of the NAV. The crimping period and the amplitude of collagen fibers reflect their ability to distend during loading. However, a shorter crimped period and a lower amplitude were observed by SHG/TPEM imaging in NAV than in HP. The differences in the degree of crimping of the collagen fibers between the two tissues are related to their physiological size and function in vivo. This specific arrangement of collagen fibers could be responsible for the distensibility of HP and NAV tissues, permitting them to stretch under load. It was observed that at 0 mmHg approximately 60% of the NAV transverse cross-sectional area has an undulating (crimping) structure [45,46]. Crimping of collagen fibers is eliminated by straightening, rotation and tautening of these fibers in the direction of the stretch axis, when the transvalvular pressure is above approximately 5 mmHg. Most of their realignment had occurred by 20 mmHg [45,46]. Previously, it was assumed that there is a correlation between the creep period and the amplitude of the col- lagen fibers in valve tissue. However, in contrast to earlier works [47,48], Stella et al. [49] tested the biaxial properties of heart valves, and concluded that their stress relaxation can be due to an internal slipping mechanism, which is probably regulated by non-collagenous components, such as GAGs. The correlation between the internal slipping mechanism and collagen creep was found to be negligible [49].

The different arrangement of the collagen fibers in the HP tissue layers may be related to the fact that the native HP works in vivo under different hemodynamic conditions than NAV. Under normal conditions, the intrapericardial pressure oscillates within the range of approximately -4/+4 mmHg during the respiratory cycle, whereas NAV is loaded by systolic/diastolic pressures of 120/80 mmHg [27,50]. In HP, the maximum stresses can be distributed between two collagen fiber-rich layers (the dense and serosal part of fibrous HP). By contrast, in NAV, lamina fibrosa forms the main load-bearing structure [51].

Elastin is accumulated on both edges of NAV, but is evenly distributed throughout HP. Elastin is responsible for the elastic properties of the NAV leaflet, and represents 13% of the total ECM dry weight [41]. Elastin is formed by lysyl oxidase crosslinking of tropoelastin monomers (~70 kDa), and it is surrounded by a fine mesh of microfibrils, predominantly fibrillin-1 and fibrillin-2 [52]. These fibrillins can bind integrins, proteoglycans and growth factors, and may play a role in cell signaling [53]. The elastin fibers in the lamina fibrosa of NAV form a highly-organized network of filaments that surround the collagen fiber bundles and stretch radially from the central region to the line of attachment of the leaflet. The elastin fibers store energy during the loading of the valve and release it to the collagen during unloading, thus allowing the valve to return to its resting position [54,55]. Elastin fibers in the ventricularis of NAV are responsible for the rapid retraction of the NAV leaflet in the radial direction during opening [41,42]. These fibers facilitate the closure movement by extending the valve leaflet as it opens, and they recoil when it closes [18,51]. They reduce the large radial strains that occur during maximum forward flow when NAV is opened. The elastin fibers in the lamina ventricularis of NAV also provide the mechanism for the pre-stress of the fibrosa by the ventricularis [18,51]. The benefit provided by this pre-stress is as yet unclear, but it is probably related to leaflet retraction. Stella et al. [49] showed that the elastin-rich ventricularis of the NAV leaflet contracted by 10.9% in the radial direction and by 8.2% in the circumferential direction, while the collagen-dominant fibrosa elongated by 28.2% in the radial direction and by 4.8% in the circumferential direction after layer separation. The elastin fibers of the lamina spongiosa are thicker in the hinge region of the NAV cusps, where they form a rectilinear pattern, as opposed to the thinner and radially oriented stripe pattern found in the middle part (belly region) of the cusps [56]. The elas- tin fibers in the lamina spongiosa probably play a role in responding to regionally specific loading patterns [56]. HP contained a smaller amount of elastin fibers than NAV. In addi- tion, the elastin fibers have a different distribution in the individual layers of the HP

tissue than in NAV. A denser concentration of elastin fibers was evident in the inner serosal part of the fibrous HP. In the HP, however, the elastin fibers were not arranged in such densely corrugated structures as were observed in the lamina ventricularis of NAV. Because of this, it can be assumed that they will have less effect on the elastic recoil and elastic recovery mechanisms in HP than in NAV. In addition, their contribution to providing the pre-stress mechanism during loading will be negligible in comparison with NAV.

The collagen I, III and elastin fibers that connect individual tissue layers are very impor- tant for the interlayer micromechanics of NAV and HP [49,57]. Considerable numbers of these transverse fibers that connect collagen and elastin fibers to each other, and bind the lamina fibrosa and lamina ventricularis together, were observed in the lamina spongiosa of NAV. In this way, the three layers of NAV are relatively closely connected, and the NAV leaflet acts as a bonded unit [45,46,49]. These connecting fibers disable physical sliding of the NAV tissue layers and maintain layer residual stresses [57]. This tissue organization enables the NAV tissue to distribute the stress between the collagen and elastin fibers and to couple the mechanics of the two layers, when the NAV cusps open and close, particularly in the low-strain flexure deformation mode [56,49]. Based on our results, the collagen I, collagen III and elastin fiber connections between the dense and serosal parts of fibrous HP were significantly weaker than the connections between the NAV tissue layers. This may be related to the lower intensity of the stress-strain loading of the HP tissue in vivo.

GAGs are formed from long unbranched chains of repeating disaccharides (N-acetylglucosamine or N-acetylgalactosamine and either uronic acid or galactose). Proteoglycans are formed when GAGs are connected by covalent linkage to a protein core [58]. GAGs (hyaluronan, heparin sulfate, chondroitin sulfate, dermatan sulfate, keratin sulfate) and proteoglycans (decorin, biglycan, versican) were found in all layers, but pref- erentially in the lamina spongiosa of the NAV leaflets. GAGs connected to fiber-fiber and fiber-matrix interactions at low force levels are able to hydrate the spongiosa layer by bind- ing water molecules by negatively-charged sulfated and carboxylated polysaccharides, and they provide viscoelasticity by dampening the vibrations. In this way, GAGs allow for the compressibility of the leaflets and permit changes in the arrangement of the collagen and of the elastic fibers in the NAV leaflet during cuspal flexure [56,59,60]. GAGs were found uniformly in all layers of the fibrous HP, but in higher amounts in the inner serosal part.

In HP and NAV tissues, the differences in the histological layers corresponded with the ECM content of collagen I, III, elastin and GAGs. Quantitative tissue analysis using an ECM-integrated density histomorphometric evaluation found that the HP contained a greater amount of collagen I, and a lower amount of collagen III and elastin than the NAV. The differences were statistically significant between the two groups ($p < 0.001$). The lower formation of elastin fibers in HP could be in relation to the physiological function, which does not require in vivo to have elastic properties that are as developed as those of NAV leaflets. Between HP and NAV tissues, no differences in GAGs content were found. The semi-quantitative evaluation of the proteins and GAGs content in the tissues can be regarded as a limiting factor for our approach. We attempted to eliminate possible mistakes by using standardized image acquisition, and the immunohistological images were evaluated by two independent evaluators.

Interactions among all components of the ECM are responsible for the biomechanical properties of the two tissues. Uniaxial tensile tests also confirmed the mechanical integrity of the HP tissue. The secant elastic modulus of the HP_L and HP_T specimens was found to be slightly higher than that of the NAV_L and NAV_R specimens. However, the differences between HP_L and NAV_L or between HP_T and NAV_R were not statistically significant, and could be the result of variability between donors. The secant elastic modulus of both tissues in the transversal or radial direction was approximately two times lower than the secant elastic modulus in the longitudinal direction. The differences between HP_L and HP_T were statistically significant ($p < 0.05$), as were the differences between NAV_L and NAV_R ($p < 0.05$). The UTS values for both tissues were also found to be higher in the longitunal direction than in the transversal or radial directions. However, the differences between the HP_L and NAV_L, and between HP_T and NAV_R, were not statistically significant. According to our results, HP exhibited non-linear and anisotropic mechanical properties similar to those of NAV. Lee

et al. [61,62] compared human and canine pericardium. They found that human pericardium was 7.3 times thicker than canine pericardium, but that it was more extensible in stress-strain tests. Sacks et al. [63] evaluated the collagen fiber architecture in bovine pericardium. They confirmed that the mechanical behavior of bovine pericardium is quantitatively consistent with its collagen fiber architecture, and the variability of the mechanical anisotropy of bovine pericardium is caused by variations in the preferred directions of the collagen fiber. Trembly et al. [64] found significant differences in stiffness and anisotropy between fresh and glutaraldehyde-fixed human or bovine pericardia, i.e. materials used in aortic arch reconstruction surgery, and healthy or dilated human ascending aorta. Fresh human pericardium was 9.5 times stiffer than healthy or dilated human ascending aortas, while fixed human pericardium was 7.1 time stiffer, and bovine pericardium was 16.4 times stiffer. Anisotropy may be related to the heterogenous and asymmetrical density and the arrangement of the collagen fibers. The Es and UTS values of both tissues may also be correlated with the crimping period and the amplitude of the collagen fibers in the tissue layers. Our UTS values for NAV are slightly higher than those published by Balquid et al. [65] (UTS 2.6 MPa for circumferential direction and 0.4 MPa for radial direction), which may be due to the higher donor age. Our UTS values for HP tissue are also higher than the UTS values reported for NAV or for tissue engineered heart valves [54]. NAV cusps were found to be stiffer in the longitudinal (circumferential) direction than in the radial direction, and a bigger collagen fiber diameter was associated with a bigger tissue stress-strain response [46,65,66]. Different NAV tissue strain magnitude values that also correlate with cusp extensibility were reported to be 70–80% in radial direction and 10–14% in the circumferential direction under 60 N/m equibiaxial tension [46,65]. Results reported by Stella and Sacks [49] indicated that even separated fibrosa and ventricularis NAV layers exhibited non-linear, highly anisotropic mechanical behavior.

Young’s elastic modulus values that reflect the anisotropy of human NAV are usually described in the range of units and tens of MPa. Balguid et al. [65] found the elastic modulus in the circumferential direction to be approximately 15 MPa, and in the radial direction the value was approximately 2 MPa for human NAV. Similar results were described by Kalejs et al., and by Strandins et al. [67,68]. Anssari-Benam et al. [69] reported that the elastic modulus of porcine NAV is 8.3 MPa in the circumferential direction and 3.9 MPa in the radial direction. Reported elastic moduli for native bovine and porcine pericardial tissue are described in the higher range of ~20–100 MPa and ~40–120 MPa, respectively [70–72]. Glutaraldehyde is used to modify natural scaffold materials by cross-linking mainly ε-amino groups of the lysyl and hydroxylysyl residues of collagen molecules. Glutaradehyde fixation further increases the elastic moduli of bovine and porcine pericardium, but the differences from the native tissue are not striking [70–72]. However, decellularization procedures using different protocols frequently produce lower elastic modulus values for bovine or porcine pericardial tissues [70–73]. TEHVs created from several biodegradable synthetic scaffolds and seeded with cells [e.g. a polyglycolic acid (PGA) scaffold coated with polyhydroxy- butyrate (PH4B) and seeded with human venous myofibroblast cells, or microfabricated poly(glycerol sebacate) (PGS) and fibrous PGS/poly(-caprolactone) (PCL) electrospun sheets seeded with sheep pulmonary VICs and MSCs] generally have a lower secant elastic modulus than human NAV and HP (~ 3–6 MPa) [54,74,75].

Flexure/bending is an important deformation mode for heart valve leaflets at low stress- low strains. They are related to the straightening of the crimped fibres of collagen and the elongation of the elastin fibers [54,76]. The bending stiffness (K) correlates with the pre-transition linear elastic phase of the stress – strain curves [54,76]. Our calculated bending stiff- ness (K) values were greater for HP_T than for HP_L and were greater for NAV_L than for NAV_R. The greater bending stiffness values for HP_T than for HP_L may be related to the dimensions of the tested samples. However, no statistically significant differences were found in the estimated bending stiffness between the two tissues in the longitudinal direction and in the transversal or radial direction. Our detected bending stiffness values for NAV tissue are in a similar range to those previously published for porcine heart valves, but our differences between the values for the circumferential and radial direction were not so large [54,77].

Preservation of the native ECM structure is very important for tissue remodeling, and all decellularization methods invariably disrupt the ECM to some degree [78]. These changes may have a negative impact on the function and the biomechanical properties of decellularized xenogeneic tissues

[70–73]. In a study by Liao et al. [79], the overall extensibility rep- resented by areal strain less than 60 N/m increased approximately two times from 68–85% for the porcine NAV to approximately 140–170% after SDS (sodium dodecyl sulphate), Trypsin or Triton X-100 decellularization. The effective flexural moduli decreased from approximately 150 kPa for the porcine NAV to 15–30 kPa for SDS, Trypsin, and Triton X-100-treated porcine NAV leaflets. Decellularization results in loss of crimping, causes substantial microscopic disruption to the collagen structure and also to the elastin layer, and causes a loss of GAGs content in the spongiosa [79]. By damaging the cells and the ECM, decellularization also disrupts the structural protection mechanism that prevents collagen from being damaged during loading [79].

The changes in the mechanical behavior and in the structural properties of decellularized heart valve leaflets may also have a negative impact on the durability of xenogeneic heart valve prostheses [80]. In addition, remnant cellular components (such as DNA, mitochondria, membrane lipids, and cytosolic proteins) can also elicit an adverse inflammatory response and inhibit constructive remodeling, if they are not adequately removed [80]. There is also an association between macrophage phenotype (a shift in macrophage phenotype predominance from M1 to M2) and remodeling outcome [80]. Several anti- gens are involved in the human immune response to xenogeneic heart valve tissue, and glutaraldehyde fixation cannot sufficiently eliminate or inactivate these foreign antigens [81]. It was confirmed that the immune response in patients towards glutaraldehyde-fixed porcine heart valves is induced by porcine proteins albumin, collagen 6A1, and also αGal epitopes (α 1,3 galactose modifications) [82]. However, there are also other non-Gal carbohydrate antigens in xenogeneic tissues, e.g. non-acid and acid glycosphingolipids. Two common sialic acids in mammals, N-acetylneuraminic acid (Neu5Ac) and its hydroxylated form N-glycolylneuraminic acid (Neu5Gc), have been described in bioprosthetic heart valves [64,65]. These xeno-antigens were recognized by human anti-Neu5Gc IgG, which supports their immunogenic nature and may play a role in valve deterioration within human patients [83,84]. Magnetic resonance imaging (MRI) and a histologocal evaluation revealed a high frequency of in vivo graft failure early after implantation, due to inflammation and fibrosis of Matrix P (a decelularized porcine graft) tissue-engineered pulmonary valves (TEPV) [85]. Surgical or transcatheter TEPV replacement was needed in 52% of patients 19 months after Matrix P TEPV implantation [85].

Even decellularized or cross-linked xenogeneic cardiovascular and reconstructive bio- materials elicit greater human immune responses than most of the allogeneic specimens tested [6]. Mirsadraee et al. [86] described how to produce an acellular human pericardial allogeneic tissue scaffold with a view to recellularization by autologous cells. Human peri- cardia from cadaveric donors were treated with a hypotonic buffer, sodium dodecyl sulfate (SDS), and a nuclease solution. There were no significant differences in the hydroxyproline (collagen) and GAGs content. However, decellularization had a negative impact on the tissue structure. There was a significant increase in the extensibility of the tissue in the direction parallel to the collagen bundles [86]. When decellularized HP tissue was seeded with dermal fibroblasts, the cells attached to the mesothelial surface, penetrated the tissue and remodeled the ECM within a week of seeding. This pericardial scaffold was observed to be biocompatible in vitro and, in the mouse model, in vivo [87]. HP tissue may therefore be capable of supporting tissue ingrowth and remodelling of cells. [88].

The current understanding of NAV geometry provides a good model design, and sufficient data are available to consider autologous glutaraldehyde fixed pericardial leaflet replacement in highly selected younger patients with irreparable leaflets and contraindications to warfarin [89]. Lausberg et al. [9] described how aortic regurgitation can be effectively treated by aortic valve repair using an autologous HP patch. A method describing the rapid fabrication of an pericardial aortic heart valve using autologous HP, which involved brief dipping in glutaraldehyde to prevent shrinkage and thickening of the untreated tis- sue, was documented in a recent report by Liu et al. in 2013 [90]. This study demonstrated a favorable functional profile and excellent haemodynamic performance (peak pressure gradient: 7.70 ± 3.41 mmHg; mean pressure gradient: 1.79 ± 0.64 mmHg) of autologous HP valve replacements in a long-term follow-up (11.43 ± 4.50 years), even in younger patients (mean age, 34 years). Only 20% of the patients required reoperation for fibrocalcific degeneration [90]. Ozaki et al. [91] demonstrated that aortic valve reconstruction is feasible using glutaraldehyde-treated autologous HP in patients with

various aortic valve diseases who are aged less than 60 years. Postoperative echocardiography revealed a normal peak gradient of 13.8 ± 3.7 mmHg 3.5 years after surgery, and freedom from reoperation was 96.2% at 53 months follow-up.

Despite these clinical trials with positive results, HP tissue is not at the present time routinely used for heart valve tissue engineering. However, it could be a very promising scaffold, due to its advantageous structure and biomechanical properties in comparison with human NAV. Minimally invasive harvesting of autologous HP tissue from an individual patient can be performed using minimally invasive (thoracoscopic) techniques or specially-designed pericardioscopic instruments. One of the functions of HP and epicardium (the outer layer of the heart, also known as visceral pericardium) is to maintain the heart in a fixed geometric position in the thorax and to limit overexpansion of the ventricles in diastole [92]. This physiological role of HP should not be affected by harvesting a small pericardial strip 10 × 4 cm in area from the anterior part of the heart, if the epicardium remains uninfluenced. This small portion of removed HP could be replaced by some kind of biodegradable material. In vitro modification of autologous HP tissue may offer a new approach for preparing an autologous and endothelialized heart valve replacement for potential clinical use in children and patients younger than 60 years who require heart valve surgery [21]. When using HP for the construction of a heart valve replacement, the anisotropy and the non-linear mechanical behavior of the tissue should be taken into account. Based on the orientation and the arrangement of the collagen fibers, the longitudinal side of the HP should correspond to the longitudinal (circumferential) side of the heart valve prosthesis, and the dense part of the fibrous HP should be localized on their outflow part. Autologous HP will also probably avoid a negative immune response that leads to the development of degenerative structural changes in heart valve replacements made from xenogeneic or biocompatible synthetic materials after in vivo implantation [93–95].

## 5. Conclusions

Our study has revealed certain similarities in the cellular structure and in the ECM structure of HP and human NAV tissues. PICs are of mesenchymal origin, as are VICs, and they were present in HP tissue predominantly in a quiescent phenotype (qPICs). The shape of live PICs, and also VICs, corresponded to the arrangement of the surrounding ECM, and was mainly related to the density of the collagen I and III fibers. Living VICs and PICs cytoplasmic filopodia formed connections and created a complex three-dimensional network between the cells, the collagen and the elastin fibers. These connections could play a role in the transfer of external mechanical stimuli from the ECM polymeric components to the cells.

We have confirmed that HP has an advantageous ECM structure and a sufficient content of essential structural proteins such as collagen I, III, elastin and GAGs in comparison with NAV. A detailed analysis of the arrangement of the collagen and elastin fibers, including an evaluation of their heterogenity in crimped periods and the amplitudes in both tissues was performed using ESEM and SHG/TPEM. Some differences were found in the stratification of the histological tissue layers. However, there was no difference between the relative thickness of the main load-bearing structure of the tissues, the dense part of the fibrous HP and the lamina fibrosa of NAV. In addition, the biomechanical properties of HP correspond to those of human NAV. The anisotropy of the HP tissue was found to be related to the arrangement of the collagen I and III fibers.

Our results indicate that HP tissue could be a promising scaffold for heart valve tissue engineering. It can be expected that a heart valve replacement made from autologous HP will have longer functional durability and a lower incidence of degenerative changes than currently-used decellularized or crosslinked xenogeneic or allogeneic heart valve substitutes. Additional research is needed to confirm these predictions.

## Disclosure statement

No potential conflict of interest was reported by the authors.

## Funding

This work was supported by the Internal Grant Agency of the Ministry of Health of the Czech Republic [grant number NT 11270 (FS, EF, LB, JP, JM)], and by the Czech Health Research Council of the Ministry of Health of the Czech Republic, [grant numbers NV15-29153A (EF, JP) and NV15-27941A (HCh, LH)].

## References

[1] Yacoub MH, Takkenberg JJ. Will heart valve tissue engineering change the world? Nat Clin Pract Cardiovasc Med. 2005;2(2):60–61.
[2] Brown JM, O'Brien SM, Wu C, et al. Isolated aortic valve replacement in North America comprising 108,687 patients in 10 years: changes in risks, valve types, and outcomes in the society of thoracic surgeons national database. J Thoracic Cardiovasc Surg. 2009;137:82–90.
[3] Cheung DY, Duan B, Butcher JT. Current progress in tissue engineering of heart valves: multiscale problems, multiscale solutions. Expert Opin Biol Ther. 2015;15(8):1155–1172.
[4] Welke KF, Wu Y, Grunkemeier GL, et al. Long-term results after Carpentier-Edwards pericardial aortic valve implantation, with attention to the impact of age. Heart Surg Forum. 2011;14(3):E160–E165.
[5] Kallio M, Pihkala J, Sairanen H, et al. Long-term results of the Ross procedure in a population- based follow-up. Eur J Cardiothorac Surg. 2015;47(5):e164–e170.
[6] Rieder E, Steinacher-Nigisch A, Weigel G. Human immune-cell response towards diverse xenogeneic and allogeneic decellularized biomaterials. Int J Surg. 2016;36(Pt A):347–351.
[7] Chester AH, Taylor PM. Molecular and functional characteristics of heart-valve interstitial cells. Philos Trans R Soc Lond B Biol Sci. 2007;362(1484):1437–1443.
[8] Rodriguez ER, Tan CD. Structure and anatomy of the human pericardium. Prog Cardiovasc Dis. 2017;59(4):327–340.
[9] Lausberg HF, Aicher D, Langer F, et al. Aortic valve repair with autologous pericardial patch. Eur J Cardiothorac Surg. 2006;2:244–249.
[10] Ozaki S, Kawase I, Yamashita H, et al. Aortic valve reconstruction using autologous pericardium for patients aged less than 60 years. J Thorac Cardiovasc Surg. 2014;148(3):934–938.
[11] Imaishi Y, Lodowski KH, Koutalos Y. Two-photon microscopy: shedding light on the chemistry of vision. Biochemistry. 2007;46(34):9674–9684.
[12] Campagnola PJ, Millard AC, Terasaki M, et al. Three-dimensional high-resolution second- harmonic generation imaging of endogenous structural proteins in biological tissues. Biophys J. 2002;82(Pt 1):493–508.
[13] Schneider CA, Rasband WS, Eliceiri KW. NIH Image to ImageJ: 25 years of image analysis. Nat Methods. 2012;9(7):671–675.
[14] Caetano GF, Fronza M, Leite MN, et al. Comparison of collagen content in skin wounds evaluated by biochemical assay and by computer-aided histomorphometric analysis. Pharm Biol. 2016;54(11):2555–2559.
[15] Fonseca C, Taatjes DJ, Callas P, et al. The effects of aging on the intimal region of the human saphenous vein: insights from multimodal microscopy and quantitative image analysis. Histochem Cell Biol. 2012;138(3):435–445.
[16] Prasad K, Prabhu GK. Image analysis tools for evaluation of microscopic views of immunohistochemically stained specimen in medical research-a review. J Med Syst. 2012;36(4):2621–2631.
[17] Frisch-Fay R. Flexible bars. Washington (DC): Butterworths; 1962.
[18] Sacks, MS, Merryman, WD, Schmidt, DE On the biomechanics of heart valve function. J. Biomech. 2009;42:1804–1824.
[19] Liu AC, Joag VR, Gotlieb AI. The emerging role of valve interstitial cell phenotypes in regulating heart valve pathobiology. Am J Pathol. 2007;171(5):1407–1418.
[20] Taylor PM, Allen SP, Yacoub MH. Phenotypic and functional characterization of interstitial cells from human heart valves, pericardium and skin. J Heart Valve Dis. 2000;9(1):150–158.
[21] Straka F, Schornik D, Masin J, et al. A new approach to heart valve tissue engineering based on modifying autologous human pericardium by 3D cellular mechanotransduction. J Biomater Tissue Eng. 2017;7:527–543.
[22] Bullwinkel J, Baron-Lühr B, Lüdemann A, et al. Ki-67 protein is associated with ribosomal RNA transcription in quiescent and proliferating cells. J Cell Physiol. 2006;206(3):624–635.
[23] Fleisher B, Clarke C, Ait-Oudhia S. Current advances in biomarkers for targeted therapy in triple-negative breast cancer. Breast Cancer (Dove Med Press). 2016;8:183–197.

[24] Latif N, Sarathchandra P, Taylor PM, et al. Characterization of molecules mediating cell-cell communication in human cardiac valve interstitial cells. Cell Biochem Biophys. 2006;45(3):255– 264.
[25] Kurpinski K, Chu J, Hashi C, et al. Anisotropic mechanosensing by mesenchymal stem cells. Proc Natl Acad Sci U S A. 2006;103(44):16095–16100.
[26] Schoen FJ. Evolving concepts of cardiac valve dynamics: the continuum of development, functional structure, pathobiology, and tissue engineering. Circulation. 2008;118(18):1864–1880.
[27] Arjunon S, Rathan S, Jo H, et al. Aortic valve: mechanical environment and mechanobiology. Ann Biomed Eng. 2013;41(7):1331–1346.
[28] Rabkin-Aikawa E, Farber M, Aikawa M, et al. Dynamic and reversible changes of interstitial cell phenotype during remodeling of cardiac valves. J Heart Valve Dis. 2004;13(5):841–847.
[29] Carruthers CA, Alfieri CM, Joyce EM, et al. Gene expression and collagen fiber micromechanical interactions of the semilunar heart valve interstitial cell. Cell Mol Bioeng. 2012;5(3):254–265.
[30] Reiser K, McCormick RJ, Rucker RB. Enzymatic and nonenzymatic cross-linking of collagen and elastin. FASEB J. 1992;6(7):2439–2449.
[31] Butcher JT, Tressel S, Johnson T, et al. Transcriptional profiles of valvular and vascular endothelial cells reveal phenotypic differences: influence of shear stress. Arterioscler Thromb Vasc Biol. 2006;26(1):69–77.
[32] Mongkoldhumrongkul N, Yacoub MH, Chester AH. Valve endothelial cells – not just any old endothelial cells. Curr Vasc Pharmacol. 2016;14(2):146–154.
[33] Chung-Welch N, Patton WF, Yen-Patton GP, et al. Phenotypic comparison between mesothelial and microvascular endothelial cell lineages using conventional endothelial cell markers, cytoskeletal protein markers and in vitro assays of angiogenic potential. Differentiation. 1989;42(1):44–53.
[34] Lachaud CC, Rodriguez-Campins B, Hmadcha A, et al. Use of mesothelial cells and biological matrices for tissue engineering of simple epithelium surrogates. Front Bioeng Biotechnol. 2015;3:117.
[35] Li S, Henry JJ. Nonthrombogenic approaches to cardiovascular bioengineering. Annu Rev Biomed Eng. 2011;13:451–475.
[36] Hristov M, Erl W, Weber PC. Endothelial progenitor cells: mobilization, differentiation, and homing. Arterioscler Thromb Vasc Biol. 2003;23(7):1185–1189.
[37] Weber B, Dijkman PE, Scherman J, et al. Off-the-shelf human decellularized tissue-engineered heart valves in a non-human primate model. Biomaterials. 2013;34(30):7269–7280.
[38] Stokes DJ. Principles and practice of variable pressure/environmental scanning electron microscopy (VP-ESEM). Chichester: Wiley; 2008.
[39] Rock CA, Han L, Doehring TC. Complex collagen fiber and membrane morphologies of the whole porcine aortic valve. PLoS One. 2014;9(1):e86087.
[40] Mega M, Marom G, Halevi R, et al. Imaging analysis of collagen fiber networks in cusps of porcine aortic valves: effect of their local distribution and alignment on valve functionality. Comput Methods Biomech Biomed Engin. 2016;19(9):1002–1008.
[41] Taylor PM. Biological matrices and bionanotechnology. Philos Trans R Soc Lond B Biol Sci. 2007;362(1484):1313–1320.
[42] Kurland NE, Drira Z, Yadavalli VK. Measurement of nanomechanical properties of biomolecules using atomic force microscopy. Micron. 2012;43(2–3):116–128.
[43] Bailey AJ, Paul RG, Knott L. Mechanisms of maturation and ageing of collagen. Mech Ageing Dev. 1998;106(1–2):1–56.
[44] Sacks MS, Smith DB, Hiester ED. The aortic valve microstructure: effects of transvalvular pressure. J Biomed Mater Res. 1998;41(1):131–141.
[45] Joyce EM, Liao J, Schoen FJ, et al. Functional collagen fiber architecture of the pulmonary heart valve cusp. Ann Thorac Surg. 2009;87(4):1240–1249.
[46] Ku CH, Johnson PH, Batten P, et al. Collagen synthesis by mesenchymal stem cells and aortic valve interstitial cells in response to mechanical stretch. Cardiovasc Res. 2006;71(3):548–556.
[47] Provenzano P, Lakes R, Keenan T, et al. Nonlinear ligament viscoelasticity. Ann Biomed Eng. 2001;29(10):908–914.
[48] Thornton GM, Frank CB, Shrive NG. Ligament creep behavior can be predicted from stress relaxation by incorporating fiber recruitment. J Rheol. 2001;45(2):493–507.
[49] Stella JA, Sacks MS. On the biaxial mechanical properties of the layers of the aortic valve leaflet. J Biomech Eng. 2007;129:757–766.
[50] Adler Y, Charron P, Imazio M, et al. ESC Guidelines for the diagnosis and management of pericardial diseases: The Task Force for the Diagnosis and Management of Pericardial Diseases of the European Society of Cardiology (ESC) Endorsed by: The European Association for Cardio- Thoracic Surgery (EACTS). Eur Heart J. 2015;36 (42):2921–64.
[51] Sacks MS, Yoganathan AP. Heart valve function: a biomechanical perspective. Philos Trans R Soc Lond B Biol Sci. 2007;29;362(1484):1369–1391.

[52] Wagenseil JE, Mecham RP. New insights into elastic fiber assembly. Birth Defects Res C Embryo Today. 2007;81(4):229–240.
[53] Bax DV, Mahalingam Y, Cain S, et al. Cell adhesion to fibrillin-1: identification of an Arg- Gly-Asp-dependent synergy region and a heparin-binding site that regulates focal adhesion formation. J Cell Sci. 2007;120(Pt 8):1383–1392.
[54] Hasan A, Ragaert K, Swieszkowski W, et al. Biomechanical properties of native and tissue engineered heart valve constructs. J Biomech. 2014;47(9):1949–1963.
[55] Isenberg BC, Williams C, Tranquillo RT. Small-diameter artificial arteries engineered in vitro. Circ Res. 2006;98:25–35.
[56] Tseng H, Grande-Allen KJ. Elastic fibers in the aortic valve spongiosa: a fresh perspective on its structure and role in overall tissue function. Acta Biomater. 2011;7(5):2101–2108.
[57] Buchanan RM, Sacks MS. Interlayer micromechanics of the aortic heart valve leaflet. Biomech Model Mechanobiol. 2014;13(4):813–826.
[58] Prydz K, Dalen KT. Synthesis and sorting of proteoglycans. J Cell Sci. 2000;113(Pt 2):193–205.
[59] Lincoln J, Lange AW, Yutzey KE. Hearts and bones: shared regulatory mechanisms in heart valve, cartilage, tendon, and bone development. Dev Biol. 2006;294(2):292–302.
[60] Eckert CE, Fan R, Mikulis B, et al. On the biomechanical role of glycosaminoglycans in the aortic heart valve leaflet. Acta Biomater. 2013;9(1):4653–4660.
[61] Lee JM, Boughner DR. Mechanical properties of human pericardium. Differences in viscoelastic response when compared with canine pericardium. Circ Res. 1985 Sep;57(3):475–481.
[62] Lee MC, Fung YC, Shabetai R, et al. Biaxial mechanical properties of human pericardium and canine comparisons. Am J Physiol. 1987 Jul;253(1 Pt 2):H75–82.
[63] Sacks MS, Chuong CJ, More R. Collagen fiber architecture of bovine pericardium. ASAIO J. 1994;40(3):M632–M637.
[64] Tremblay D, Zigras T, Cartier R, et al. A comparison of mechanical properties of materials used in aortic arch reconstruction. Ann Thorac Surg. 2009 Nov;88(5):1484–1491.
[65] Balguid A, Rubbens MP, Mol A, et al. The role of collagen cross-links in biomechanical behavior of human aortic heart valve leaflets–relevance for tissue engineering. Tissue Eng. 2007;13(7):1501–1511.
[66] Christie GW, Barratt-Boyes BG. Mechanical properties of porcine pulmonary valve leaflets: how do they differ from aortic leaflets? Ann Thorac Surg.1995;60(2Suppl):S195–S199.
[67] Kalejs M, Stradins P, Lacis R, et al. St Jude Epic heart valve bioprostheses versus native human and porcine aortic valves – comparison of mechanical properties. Interact Cardiovasc Thorac Surg. 2009;8(5):553–556.
[68] Stradins P, Lacis R, Ozolanta I, et al. Comparison of biomechanical and structural properties between human aortic and pulmonary valve. Eur J Cardio-Thorac Surg. 2004;26:634–639.
[69] Anssari-Benam A, Bader DL, Screen HR. A combined experimental and modelling approach to aortic valve viscoelasticity in tensile deformation. J Mater Sci Mater Med. 2011;22(2):253–262.
[70] Sung HW, Chang Y, Chiu CT, et al. Crosslinking characteristics and mechanical properties of a bovine pericardium fixed with a naturally occurring crosslinking agent. J Biomed Mater Res. 1999;47(2):116–126.
[71] Zioupos P, Barbenel JC. Mechanics of native bovine pericardium. I. The multiangular behaviour of strength and stiffness of the tissue. Biomaterials. 1994;15(5):366–373.
[72] Aguiari P, Fiorese M, Iop L, et al. Mechanical testing of pericardium for manufacturing prosthetic heart valves. Interact Cardiovasc Thorac Surg. 2016;22(1):72–84.
[73] Cissell DD, Hu JC, Griffiths LG, et al. Antigen removal for the production of biomechanically functional, xenogeneic tissue grafts. J Biomech. 2014;47(9):1987–1996.
[74] Balguid A, Driessen NJ, Mol A, et al. Stress related collagen ultrastructure in human aortic valves-implications for tissue engineering. J Biomech. 2008;41(12):2612–2617.
[75] Masoumi N, Annabi N, Assmann A, et al. Tri-layered elastomeric scaffolds for engineering heart valve leaflets. Biomaterials. 2014;35(27):7774–7785.
[76] Merryman WD, EngelmayrGC, Liao, J, et al. Defining biomechanical endpoints for tissue engineered heart valve leaflets from native leaflet properties. Progress Pediatric Cardiol. 2006;21(21):153–160.
[77] Gloeckner DC, Billiar KL, Sacks MS. Effects of mechanical fatigue on the bending properties of the porcine bioprosthetic heart valve. ASAIO J. 1999;45(1):59–63.
[78] Keane TJ, Swinehart IT, Badylak SF. Methods of tissue decellularization used for preparation of biologic scaffolds and in vivo relevance. Methods. 2015;84:25–34.
[79] Liao J, Joyce EM, Sacks MS. Effects of decellularization on the mechanical and structural properties of the porcine aortic valve leaflet. Biomaterials. 2008;29(8):1065–1074.
[80] Keane TJ, Londono R, Turner NJ, et al. Consequences of ineffective decellularization of biologic scaffolds on the host response. Biomaterials. 2012;33(6):1771–1781.

[81] Bloch O, Golde P, Dohmen PM, et al. Immune response in patients receiving a bioprosthetic heart valve: lack of response with decellularized valves. Tissue Eng Part A. 2011;17(19–20):2399–2405.
[82] Böer U, Buettner FFR, Schridde A, et al. Antibody formation towards porcine tissue in patients implanted with crosslinked heart valves is directed to antigenic tissue proteins and αGal epitopes and is reduced in healthy vegetarian subjects. Xenotransplantation. 2017;24(2). doi: 10.1111/xen.12288.
[83] Barone A, Benktander J, Teneberg S, et al. Characterization of acid and non-acid glycosphingolipids of porcine heart valve cusps as potential immune targets in biological heart valve grafts. Xenotransplantation. 2014;21(6):510–522.
[84] Reuven EM, Leviatan Ben-Arye S, Marshanski T, et al. Characterization of immunogenic Neu5Gc in bioprosthetic heart valves. Xenotransplantation. 2016;23(5):381–392.
[85] Voges I, Bräsen JH, Entenmann A, et al. Adverse results of a decellularized tissue-engineered pulmonary valve in humans assessed with magnetic resonance imaging. Eur J Cardiothorac Surg. 2013;44(4):e272–e279.
[86] Mirsadraee S, Wilcox HE, Korossis SA, et al. Development and characterization of an acellular human pericardial matrix for tissue engineering. Tissue Eng. 2006;12(4):763–773.
[87] Mirsadraee S, Wilcox HE, Watterson KG, et al. Biocompatibility of acellular human pericardium. J Surg Res. 2007;143(2):407–414.
[88] Vinci MC, Tessitore G, Castiglioni L, et al. Mechanical compliance and immunological compatibility of fixative-free decellularized/cryopreserved human pericardium. PLoS One. 2013;8(5):e64769.
[89] Rankin JS, Nöbauer C, Crooke PS, et al. Techniques of autologous pericardial leaflet replacement for aortic valve reconstruction. Ann Thorac Surg. 2014;98(2):743–745.
[90] Liu X, Han L, Song Z, et al. Aortic valve replacement with autologous pericardium: long- term follow-up of 15 patients and in vivo histopathological changes of autologous pericardium. Interact Cardiovasc Thorac Surg. 2013;16(2):123–128.
[91] Ozaki S, Kawase I, Yamashita H, et al. Aortic valve reconstruction using autologous pericardium for patients aged less than 60 years. J Thorac Cardiovasc Surg. 2014;148(3):934–8.
[92] Jöbsis PD, Ashikaga H, Wen H, et al. The visceral pericardium: macromolecular structure and contribution to passive mechanical properties of the left ventricle. Am J Physiol Heart Circ Physiol. 2007;293(6):H3379–H3387.
[93] Siddiqui RF, Abraham JR, Butany J. Bioprosthetic heart valves: modes of failure. Histopathology. 2009;55(2):135–144.
[94] Jamieson WR, Rosado LJ, Munro AI, et al. Carpentier-Edwards standard porcine bioprosthesis: primary failure (structural valve deterioration) by age groups. Ann. Thorac. Surg. 1988;46(2):155– 162.
[95] Wong ML, Wong JL, Vapniarsky N, et al. In vivo xenogeneic scaffold fate is determined by residual antigenicity and extracellular matrix preservation. Biomaterials. 2016;92:1–12.